

# REPORT DOCUMENTATION PAGE

*Form Approved*  
**OMB No. 0704-0188**

Public reporting burden for this collection of information is estimated to average 1 hour per response, including the time for reviewing instructions, searching existing data sources, gathering and maintaining the data needed, and completing and reviewing this collection of information. Send comments regarding this burden estimate or any other aspect of this collection of information, including suggestions for reducing this burden to Department of Defense, Washington Headquarters Services, Directorate for Information Operations and Reports (0704-0188), 1215 Jefferson Davis Highway, Suite 1204, Arlington, VA 22202-4302. Respondents should be aware that notwithstanding any other provision of law, no person shall be subject to any penalty for failing to comply with a collection of information if it does not display a currently valid OMB control number. **PLEASE DO NOT RETURN YOUR FORM TO THE ABOVE ADDRESS.**

|  |                                    |  |                                   |  |  |
|--|------------------------------------|--|-----------------------------------|--|--|
| <b>1. REPORT DATE (DD-MM-YYYY)</b><br>20-03-2003   |                                    | <b>2. REPORT TYPE</b><br>Technical Paper   |                                   | <b>3. DATES COVERED (From - To)</b>                              |  |
| <b>4. TITLE AND SUBTITLE</b><br><br>Infrared Spectra of Aluminum Hydrides in Solid Hydrogen: Al <sub>2</sub> H <sub>4</sub> and Al <sub>2</sub> H <sub>6</sub> |                                    |  |                                   | <b>5a. CONTRACT NUMBER</b>                                       |  |
|  |                                    |  |                                   | <b>5b. GRANT NUMBER</b>  |  |
|  |                                    |  |                                   | <b>5c. PROGRAM ELEMENT NUMBER</b>                                |  |
| <b>6. AUTHOR(S)</b><br><br>Xuefeng Wang, Lester Andrews <sup>1</sup> Simon Tam, Michelle E. DeRose, Mario E. Fajardo   |                                    |  |                                   | <b>5d. PROJECT NUMBER</b><br>2303                                |  |
|  |                                    |  |                                   | <b>5e. TASK NUMBER</b><br>M2C8                                   |  |
|  |                                    |  |                                   | <b>5f. WORK UNIT NUMBER</b>                                      |  |
| <b>7. PERFORMING ORGANIZATION NAME(S) AND ADDRESS(ES)</b>  |                                    |  |                                   | <b>8. PERFORMING ORGANIZATION REPORT NUMBER</b>                  |  |
| <sup>1</sup> Department of Chemistry<br>P.O. Box 400319<br>University of Virginia<br>Charlottesville, VA 22904-4319  |                                    | <sup>2</sup> Air Force Research Laboratory<br>AFRL/PRS<br>10 E. Saturn Blvd.<br>Edwards AFB, CA 93524-7680 |                                   | AFRL-PR-ED-TP-2003-037   |  |
| <b>9. SPONSORING / MONITORING AGENCY NAME(S) AND ADDRESS(ES)</b>   |                                    |  |                                   |  |  |
| Air Force Research Laboratory (AFMC)<br>AFRL/PRS<br>5 Pollux Drive<br>Edwards AFB CA 93524-7048  |                                    |  |                                   | <b>10. SPONSOR/MONITOR'S ACRONYM(S)</b>                          |  |
|  |                                    |  |                                   | <b>11. SPONSOR/MONITOR'S NUMBER(S)</b><br>AFRL-PR-ED-TP-2003-037 |  |
| <b>12. DISTRIBUTION / AVAILABILITY STATEMENT</b><br><br>Approved for public release; distribution unlimited.   |                                    |  |                                   |  |  |
| <b>13. SUPPLEMENTARY NOTES</b>   |                                    |  |                                   |  |  |
| <b>14. ABSTRACT</b>  |                                    |  |                                   |  |  |
| 20040224 092   |                                    |  |                                   |  |  |
| <b>15. SUBJECT TERMS</b>   |                                    |  |                                   |  |  |
| <b>16. SECURITY CLASSIFICATION OF:</b>   |                                    |  | <b>17. LIMITATION OF ABSTRACT</b> | <b>18. NUMBER OF PAGES</b>                                       | <b>19a. NAME OF RESPONSIBLE PERSON</b>                             |
| <b>a. REPORT</b><br>Unclassified   | <b>b. ABSTRACT</b><br>Unclassified | <b>c. THIS PAGE</b><br>Unclassified  | A                                 | 42   | Leilani Richardson   |
|  |                                    |  |                                   |  | <b>19b. TELEPHONE NUMBER (include area code)</b><br>(661) 275-5015 |

Standard Form 298 (Rev. 8-98)  
Prescribed by ANSI Std. Z39.18

## Best Available Copy

# Infrared Spectra of Aluminum Hydrides in Solid Hydrogen: $\text{Al}_2\text{H}_4$ and $\text{Al}_2\text{H}_6$

Xuefeng Wang and Lester Andrews\*

*Department of Chemistry, P. O. Box 400319, University of Virginia*

*Charlottesville, VA 22904-4319*

Simon Tam<sup>a</sup>, Michelle E. DeRose, and Mario E. Fajardo<sup>b</sup>

*U.S. Air Force Research Laboratory, AFRL/PRSP, Edwards AFB, CA 93524-7680*

The reaction of laser-ablated Al atoms and normal- $\text{H}_2$  during co-deposition at 3.5 K produces  $\text{AlH}$ ,  $\text{AlH}_2$ , and  $\text{AlH}_3$  based on infrared spectra, and the results of isotopic substitution ( $\text{D}_2$ ,  $\text{H}_2 + \text{D}_2$  mixtures,  $\text{HD}$ ). Four new bands are assigned to  $\text{Al}_2\text{H}_4$  from annealing, photochemistry, and agreement with frequencies calculated using density functional theory. Ultraviolet photolysis markedly increases the yield of  $\text{AlH}_3$  and seven new absorptions for  $\text{Al}_2\text{H}_6$  in the infrared spectrum of the solid hydrogen sample. These seven vibrational frequencies include terminal  $\text{Al-H}_2$  and bridge  $\text{Al-H-Al}$  stretching and  $\text{AlH}_2$  bending modes, which are accurately predicted by quantum chemical calculations for dibridged  $\text{Al}_2\text{H}_6$ , a molecule isostructural with diborane. Annealing these samples to remove the  $\text{H}_2$  matrix decreases the sharp  $\text{AlH}_3$  and  $\text{Al}_2\text{H}_6$  absorptions and forms broad  $1720 \pm 20$  and  $720 \pm 20 \text{ cm}^{-1}$  bands, which are due to solid  $(\text{AlH}_3)_n$  formed on the CsI window. Complementary experiments with thermal Al atoms and para- $\text{H}_2$  at 2.4 K give similar spectra and most product frequencies within  $2 \text{ cm}^{-1}$ . Although many volatile binary boron hydride compounds are known, binary aluminum hydride chemistry is limited to the polymeric  $(\text{AlH}_3)_n$  solid. Our experimental characterization of the dibridged  $\text{Al}_2\text{H}_6$  molecule provides an important link between the chemistries of boron and aluminum.

---

\* - To whom correspondence should be addressed. E-mail: lsa@virginia.edu.

a - Present Address: KLA-Tencor Corp., 1 Technology Drive, Milpitas, CA 95035

b - Present Address: U.S. Air Force Research Laboratory, AFRL/MNME, Eglin AFB, FL

32542-5910

## Introduction

Boron hydride chemistry has been investigated for a century and a large number of distinct boron hydride compounds have been identified and characterized;<sup>1-4</sup> however, aluminum hydride chemistry under normal conditions is limited to the volatile polymeric solid trihydride  $(\text{AlH}_3)_n$ .<sup>4-6</sup> The diborane molecule is fundamentally important and the textbook example of hydrogen ( $\mu$ -hydrido) bridge bonding.<sup>4</sup> Although the isostructural dialane molecule is calculated to be stable by several groups,<sup>7-13</sup> molecular  $\text{Al}_2\text{H}_6$  has not been isolated even though the binding energy for dialane is calculated to be slightly smaller than that for diborane but significantly larger than computed for digallane.<sup>8,10</sup> The failure to observe dialane is even more surprising in view of the recent synthesis of digallane, which yielded an isostructural  $\text{Ga}_2\text{H}_6$  molecule and a polymeric solid.<sup>14-16</sup> However, the properties of solid gallane suggest a discrete oligomer, such as  $(\text{GaH}_3)_4$ , which retains terminal M-H bonds,<sup>16</sup> unlike solid  $(\text{AlH}_3)_n$ , which contains only Al-H-Al bridge bonds.<sup>5</sup> The only experimental evidence for  $\text{Al}_2\text{H}_6$  is mass spectrometric detection of trace  $\text{Al}_2\text{H}_6^+$  cation<sup>17-19</sup> and a broad photodetachment spectrum of  $\text{Al}_2\text{H}_6^-$  anion.<sup>20</sup> Surface science investigations suggest that aluminum hydrides such as  $\text{AlH}$ ,  $\text{AlH}_3$ , and  $\text{Al}_2\text{H}_6$  desorb at elevated temperatures from Al metal surfaces containing  $(\text{AlH}_3)_n$  or adsorbed hydrogen.<sup>18-22</sup>

Since the dimerization of  $\text{AlH}_3$  is exothermic by about 35 kcal/mol depending on the theoretical methods employed,<sup>8,10,11,21</sup> the direct  $\text{Al}_2\text{H}_6$  preparation involves dimerization of  $\text{AlH}_3$ . Alane ( $\text{AlH}_3$ ) has been observed by three groups from reactions of energetic aluminum atoms with hydrogen in solid argon and characterized by infrared spectroscopy,<sup>23-26</sup> however, the concentration of  $\text{AlH}_3$  was not sufficient to form  $\text{Al}_2\text{H}_6$  in the rigid argon matrix. Our successful synthesis of  $\text{Al}_2\text{H}_6$  for the first time involves pure hydrogen as the matrix.<sup>27-29</sup> This ensures the selective formation of the highest monohydride  $\text{AlH}_3$ , and diffusion on annealing the soft hydrogen matrix to

6.5 K allows dimerization to  $\text{Al}_2\text{H}_6$ . Similar laser ablation experiments with boron and hydrogen give  $\text{B}_2\text{H}_6$ .<sup>30,31</sup>

### Experimental and Theoretical Methods

The experiment for reaction of laser-ablated aluminum atoms with hydrogen during condensation in excess argon and neon have been described previously.<sup>23,30,32,33</sup> The Nd:YAG laser fundamental (1064 nm, 10 Hz repetition rate with 10 ns pulse width) was focused (10 cm f.l. lens) onto a rotating aluminum target (Johnson Matthey, 99.998%). The laser energy was varied from 10-20 mJ/pulse at the sample. Laser-ablated aluminum atoms were co-deposited with 60 STPcc of pure normal hydrogen or deuterium (Matheson) or 120 STPcc of  $\text{Ne}/\text{H}_2$  or  $\text{Ne}/\text{D}_2$  onto a 3.5 K CsI cryogenic window for 25-30 min or for 50-60 min. Mixed isotopic HD (Cambridge Isotopic Laboratories) and  $\text{H}_2 + \text{D}_2$  samples were used in different experiments. FTIR spectra were recorded at  $0.5 \text{ cm}^{-1}$  resolution on Nicolet 750 with  $0.1 \text{ cm}^{-1}$  accuracy using an MCTB detector. Matrix samples were annealed at different temperatures using resistance heat, and selected samples were subjected to filtered broadband photolysis by a medium pressure mercury arc lamp (Phillips, 175W) with globe removed for 20 min periods.

Complementary thermal Al experiments in para- $\text{H}_2$  were performed at Edwards AFB. Samples were prepared by codeposition of Al atoms from a commercial thermal effusive source (EPI SUMO) and a fast flow of precooled para- $\text{H}_2$  gas<sup>34</sup> onto a  $\text{BaF}_2$  substrate cooled to  $T \approx 2 \text{ K}$  in a liquid helium bath cryostat.<sup>35</sup> Operation of the ortho/para converter at  $T = 15 \text{ K}$  yields  $\approx 100$  ppm residual ortho- $\text{H}_2$  content. Infrared absorbance spectra,  $\log_{10}(I_0/I)$ , were recorded with a Bruker IFS120HR spectrometer at resolutions of  $0.02$  to  $0.1 \text{ cm}^{-1}$ ; sample thickness and dopant concentrations are calculated from these spectra as described previously.<sup>36</sup> Ultraviolet absorption spectra (not shown) were recorded during some sample depositions, resulting in very

weak irradiation and the consequent appearance of minor photolysis products in the as-deposited samples. Samples were deliberately photolyzed in the ultraviolet using an unfiltered 30W deuterium lamp located  $\approx 8$  cm from the deposition substrate.

Density functional theory (DFT) calculations of aluminum hydride frequencies are given for comparison with experimental values. The Gaussian 98 program<sup>37</sup> was employed with the 6-311++G\*\* basis set for hydrogen and aluminum.<sup>38,39</sup> All geometrical parameters were fully optimized with the B3LYP and BPW91 density functionals,<sup>40-44</sup> and analytical vibrational frequencies were obtained at the optimized structures.

## Results

Laser-ablated Al atoms were co-deposited with pure hydrogen, neon/H<sub>2</sub>, and argon/H<sub>2</sub> samples, and new infrared absorptions will be presented along with supporting density functional calculations of aluminum hydrides.

**Hydrogen.** Aluminum atoms were co-deposited with pure normal hydrogen using three different laser energies and different sample irradiations: spectra from the lowest laser energy investigations are illustrated in Figure 1. The spectrum of the deposited sample is dominated by the strong AlH absorption at 1598.7 cm<sup>-1</sup>, which is intermediate between the gas phase (1624.4 cm<sup>-1</sup>)<sup>45,46</sup> and argon matrix (1590.7 cm<sup>-1</sup>) absorptions<sup>23-25,47</sup> for diatomic AlH. Absorptions are also observed for AlH<sub>3</sub> (1883.7, 782.9, 712.2 cm<sup>-1</sup>) and AlH<sub>2</sub> (1821.9, 1878.9 cm<sup>-1</sup>), which are approximately 1, 0, 14 cm<sup>-1</sup> and 16, 28 cm<sup>-1</sup> higher than argon matrix values.<sup>23-26</sup> New absorptions are observed at 1838.4, 1835.8, 1825.5, 747 cm<sup>-1</sup> (labeled Al<sub>2</sub>H<sub>4</sub>), at 1638.1 cm<sup>-1</sup> (labeled AlH<sub>4</sub><sup>-</sup>),<sup>48</sup> at 1156.1 cm<sup>-1</sup> (labeled Al<sub>2</sub>H<sub>2</sub>)<sup>23</sup> with the hint of very weak absorptions at 1932.3, 1915.1, 1408.1, 1268.2, 835.6, 702.4, 631.9 cm<sup>-1</sup> (labeled DA) (Fig. 1a). Annealing to 6.2 K increased all bands except AlH and AlH<sub>4</sub><sup>-</sup> (Fig. 1b). Photolysis stepwise at  $\lambda > 380, 290, 240$  nm destroyed the Al<sub>2</sub>H<sub>2</sub>

absorption, decreased the AlH band, and increased the AlH<sub>3</sub> absorptions 2×, 6× and 13× and the DA band set 2×, 4× and 16× (Fig. 1 c,d,e). A subsequent annealing to 6.5 K increased all but the 1638 cm<sup>-1</sup> band (Fig. 1f), and a final  $\lambda > 240$  nm irradiation increased the DA bands another 25% (Fig. 1g). These experiments were remarkably free of oxide impurities: Al<sub>2</sub>O was typically A < 0.001 at 995.2 cm<sup>-1</sup> on deposition<sup>31</sup> and HO<sub>2</sub> was not detected.<sup>49</sup>

Similar behavior was found in the other hydrogen experiments. Although irradiation at  $\lambda > 630$  nm had no discernable effect,  $\lambda > 530$  nm photolysis destroyed the 1156.1 cm<sup>-1</sup> band, slightly decreased AlH<sub>2</sub> bands, slightly increased Al<sub>2</sub>H<sub>4</sub> and DA bands, and left the sharp 844.1 cm<sup>-1</sup> band unchanged. Irradiation at  $\lambda > 380$  nm slightly decreased Al<sub>2</sub>H<sub>4</sub> peaks and markedly decreased AlH<sub>2</sub>, whereas  $\lambda > 240$  nm virtually destroyed Al<sub>2</sub>H<sub>4</sub> with significant increases in AlH<sub>3</sub> and DA absorptions (Fig. 2). Another spectrum after  $\lambda > 240$  nm photolysis is shown in Fig. 3a including the solid hydrogen absorptions at 4220 and 4149 cm<sup>-1</sup>. Annealing to 6.8 K allows H<sub>2</sub> to evaporate: solid H<sub>2</sub> absorptions, AlH<sub>3</sub> bands and DA absorptions decrease by 80-90%, and broad absorptions appear at 1720 ±20 and 720±20 cm<sup>-1</sup> (Fig. 3b). Further annealing to 7.0 K allows all H<sub>2</sub> to evaporate, all sharp absorptions disappear, and the broad absorptions remain (Fig. 3c). These broad bands decrease steadily on annealing to room temperature where 30% of the broad absorbance remains.

Al atoms and D<sub>2</sub> were co-deposited in three experiments, and the spectrum from the sample using higher laser energy is shown in Figure 4. The AlD<sub>x</sub> product absorptions observed on deposition include AlD<sub>3</sub>, Al<sub>2</sub>D<sub>4</sub>, AlD<sub>2</sub> and AlD as listed in Table 1. The DA peaks appear on  $\lambda > 290$  nm photolysis, increase markedly on  $\lambda > 240$  nm irradiation, and increase slightly on subsequent 8.0 K annealing (Fig. 4 c,e,f). One difference: new bands at 1050.0, 1043.0 cm<sup>-1</sup> with

D<sub>2</sub> have no H<sub>2</sub> counterparts. On  $\lambda > 290$  nm photolysis, these bands give way to the 1183.2 cm<sup>-1</sup> counterpart (AlD<sub>4</sub><sup>-</sup>) of the 1638.1 cm<sup>-1</sup> absorption in solid hydrogen. Further annealing to 9.0 K increases Al<sub>2</sub>D<sub>4</sub> bands twofold with a small decrease in AlD<sub>2</sub> absorptions (Fig. 4g). Note that solid D<sub>2</sub> can be annealed about 3 K warmer than solid H<sub>2</sub> before the solid evaporates. Annealing to 9.3 K reveals decreased sharp product absorptions, annealing to 10.2 K markedly decreases solid D<sub>2</sub> bands at 3286, 3168, 2982 cm<sup>-1</sup> and the new product bands, and produces a broad 1260±20 cm<sup>-1</sup> absorption. Further annealing to 14 K leaves the broad band with weak CH<sub>4</sub>, CO and CO<sub>2</sub> peaks (Fig. 3e). At about 50 K CH<sub>4</sub> and CO evaporate leaving the broad 1260±20 cm<sup>-1</sup> band and CO<sub>2</sub>. This broad band decreases on warming to 290 K where about 50% remains on the CsI sample window.

Three experiments were done with different H<sub>2</sub> + D<sub>2</sub> mixtures, and the Al-H and Al-D regions reveal strong bands in the spectrum of a 35% H<sub>2</sub> + 65% D<sub>2</sub> sample; detail from the Al-H region is shown in Fig. 2d. Slight shifts in peaks are due to the change from pure H<sub>2</sub>, but several new absorptions arise from isotopic mixing. As the matrix host evaporates at 9-10 K, the sharp product absorptions decrease, and broad bands appear, and on annealing to 13 K the broad bands remain at 1740±20, 1280±20, and 710±20 on the salt window (Fig. 3f). One experiment was performed with pure HD, and the 1950-1150 cm<sup>-1</sup> region is illustrated in Figure 5. More detail is shown in Fig. 2 e,f, where four new, sharp bands were observed near 1920 cm<sup>-1</sup>.

Thermal aluminum atoms were codeposited with para-H<sub>2</sub> at 2.4 K using Al concentrations ranging from 7 to 100 ppm. Spectra from the most dilute sample are shown in Figure 6 where the product bands are weak: AlH is dominant at 1606.0 cm<sup>-1</sup>. Warming to 4.8 K increased weak 1840.9, 1838.3, 1826.8 cm<sup>-1</sup> (Al<sub>2</sub>H<sub>4</sub>) and 1155.0 cm<sup>-1</sup> (Al<sub>2</sub>H<sub>2</sub>) bands, and ultraviolet photolysis for 10 min produced new 1885.5, 1825.0, 1822.0, 1790.2, 1787.9 cm<sup>-1</sup> absorptions (labeled AlH<sub>3</sub> and

AlH<sub>2</sub>), markedly increased AlH (1618.4, 1606.0 cm<sup>-1</sup>), and destroyed the 1155.0 cm<sup>-1</sup> band. All of these absorption features show complicated reversible temperature dependences, possibly due to the reversible formation of ortho-H<sub>2</sub>/dopant clusters; however, this hypothesis is still under investigation and will be discussed elsewhere.<sup>50</sup> Of significance here is the fact that the main absorption features in solid para-H<sub>2</sub> all appear within  $\pm 2$  cm<sup>-1</sup> of the corresponding absorptions in a normal-H<sub>2</sub> host. A similar experiment with 100 ppm Al produced stronger Al<sub>2</sub>H<sub>4</sub> bands on deposition (Fig. 7a). A longer ultraviolet photolysis produced strong AlH<sub>3</sub> and AlH bands and weak DA bands at 1933.5, 1918.6, 1406.1, 1264.3 (Fig. 7b), and 835.2 cm<sup>-1</sup> (the BaF<sub>2</sub> substrate reduces the reliability of spectra below  $\approx 800$  cm<sup>-1</sup>). Annealing to 4.8 K for 60 min slightly increased the product absorptions (Fig. 7c). Finally, high resolution spectra are shown in the 1950-1750 cm<sup>-1</sup> region in Figure 8. This thinner sample was deposited in only 30 min and so received much less ultraviolet pre-irradiation, thus much weaker bands are observed on sample deposition at 2.4 K (Fig. 8a), and the growth of AlH<sub>3</sub>, AlH<sub>2</sub>, and AlH bands is obvious on photolysis (Fig. 8b). Of most interest is the "clean" spectrum recorded during annealing at 4.6 K (Fig. 8c), which reveals a sharp dominant 1885.5 cm<sup>-1</sup> AlH<sub>3</sub> absorption, sharp Al<sub>2</sub>H<sub>4</sub> bands at 1840.9, 1838.3, 1826.8 cm<sup>-1</sup>, sharp AlH<sub>2</sub> bands at 1822.0, 1787.9 cm<sup>-1</sup>, and DA bands at 1933.6, 1918.6 cm<sup>-1</sup>. A sharp Al<sub>2</sub>H<sub>4</sub> band is also observed at 747.8 cm<sup>-1</sup>.

**Neon.** Neon matrix investigations were performed with high hydrogen concentrations to favor higher hydrides. Figure 9 illustrates spectra from a Ne/10% H<sub>2</sub> experiment. The strong absorptions in the first spectrum at 1889.1 and 1828.6 cm<sup>-1</sup> (Fig. 9a) are immediately recognized as AlH<sub>3</sub> and AlH<sub>2</sub> from their blue shifts relative to hydrogen and argon matrix absorptions for these molecules. Weak absorptions at 1931.4, 1923.1, 1404.7, and 1260.2 cm<sup>-1</sup> (labeled DA) in the first

spectrum increase on photolysis and annealing (Fig. 9 b,c,d). The deuterium counterparts from a similar Ne/10% D<sub>2</sub> experiment are listed in Table 1.

**Argon.** Argon matrix experiments were done with 10% H<sub>2</sub> to compare with the present neon and earlier argon/dilute H<sub>2</sub> work. Product absorptions in the deposited spectrum (Table 1) are in agreement with previous assignments to AlH<sub>3</sub>, AlH<sub>2</sub>, AlH<sub>4</sub><sup>-</sup> and AlH in solid argon.<sup>23-26,47,48</sup> Neither HO<sub>2</sub> nor AlO<sub>2</sub> absorptions were detected, but a weak Al<sub>2</sub>O band was observed at 992.4 cm<sup>-1</sup>.<sup>32,49</sup> Satellite absorptions at 1811.8 and 1777.3 cm<sup>-1</sup> are appropriate for the (H<sub>2</sub>)AlH<sub>2</sub> complex.<sup>23,25</sup> Annealing to 10-12 K had little effect on the spectrum. Irradiation at  $\lambda > 290$  nm decreased AlH<sub>2</sub> and AlH bands but increased AlH<sub>3</sub> and AlH<sub>4</sub><sup>-</sup> absorptions. Subsequent annealing to 16 K increased absorptions at 1822.8 and 1812.0 cm<sup>-1</sup> and produced weak new bands at 1922.2, 1388.0 and 1243.4 cm<sup>-1</sup>. Subsequent  $\lambda > 240$  nm irradiation and 23 K annealing continued these trends.

**Calculations.** Density functional calculations were performed at the B3LYP/6-311++G\*\* level to provide a consistent set of frequencies for aluminum hydrides and their partially and fully deuterated counterparts to assist in the identification of the new Al<sub>2</sub>H<sub>4</sub> and Al<sub>2</sub>H<sub>6</sub> molecules observed here. Our results are presented in Tables 2 and 3. The frequencies and bond lengths computed for AlH<sub>2</sub>, AlH<sub>3</sub>, and AlH<sub>4</sub><sup>-</sup> are in line with previous calculations.<sup>23-26,48</sup> We also find AlH<sub>2</sub><sup>-</sup> to be a stable anion with lower frequencies than AlH<sub>4</sub><sup>-</sup>.

Our B3LYP calculations reach the same conclusions about Al<sub>2</sub>H<sub>4</sub> isomers as the previous investigation.<sup>51</sup> It is necessary to have infrared intensities to identify the Al<sub>2</sub>H<sub>4</sub> isomer formed here (Table 2).

The important Al<sub>2</sub>H<sub>6</sub> molecule has attracted considerable theoretical attention, and these calculations reveal a stable molecule of D<sub>2h</sub> symmetry and frequencies in accord with this

structure.<sup>7-13</sup> Table 3 compares the infrared active modes computed at SCF, CCSD, B3LYP and BPW91 levels of theory, and shows how the calculated frequencies decrease in this order. Figure 10 illustrates the B3LYP structure for Al<sub>2</sub>H<sub>6</sub>, which is in agreement with previous reports<sup>7-13</sup> and is useful to picture the vibrational modes.

## Discussion

The new absorptions observed here will be assigned to the Al<sub>2</sub>H<sub>4</sub> and Al<sub>2</sub>H<sub>6</sub> molecules on the basis of their reactions on annealing, photochemistry, behavior on deuterium substitution, and comparison to vibrational frequencies predicted by density functional calculations. This work provides the first experimental evidence for these two neutral dialane molecules.

**Al<sub>2</sub>H<sub>4</sub>.** The 1840-1780 cm<sup>-1</sup> region of our normal hydrogen matrix spectra contains five sharp peaks. The strongest band at 1821.9 cm<sup>-1</sup> is associated with the 1787.8 cm<sup>-1</sup> band on annealing and photolysis throughout these experiments: these major product bands are 15.9 and 18.2 cm<sup>-1</sup> above argon matrix AlH<sub>2</sub> bands<sup>23,25</sup> and 6.7 and 6.9 cm<sup>-1</sup> below new neon matrix AlH<sub>2</sub> bands observed here. This is the relationship found for neon, hydrogen and argon matrix absorptions of the same species.<sup>49</sup> The much larger argon-to-hydrogen matrix shifts for AlH<sub>2</sub> compared to AlH<sub>3</sub> (1 cm<sup>-1</sup>) suggests that AlH<sub>2</sub> in solid hydrogen may in fact be a weak (H<sub>2</sub>)AlH<sub>2</sub> complex;<sup>23,25</sup> however the 1821.9 and 1787.8 cm<sup>-1</sup> bands are sharp, and we find no evidence of an associated H-H stretching mode. In para-H<sub>2</sub>, these bands are at 1822.0 and 1787.9 cm<sup>-1</sup>. A weaker, sharp 770.5 cm<sup>-1</sup> band appears to be due to the bending mode of AlH<sub>2</sub> observed at 766.4 cm<sup>-1</sup> in solid argon.<sup>25</sup>

The sharp 1838.4, 1835.8, and 1825.5 cm<sup>-1</sup> bands behave as a group on annealing and photolysis. The  $\lambda > 530$  and 470 nm photolysis sequence decreased AlH<sub>2</sub> absorptions and slightly increased the above group whereas  $\lambda > 290$  nm reversed this trend and  $\lambda > 240$  nm almost destroyed

both band sets. The  $\lambda > 380$  photolysis slightly decreased the above group but nearly destroyed the  $\text{AlH}_2$  absorptions (Fig. 2b). The unique nature of these sharp bands is demonstrated by their spontaneous formation on deposition in para- $\text{H}_2$  at 1840.9, 1838.3, and 1826.8  $\text{cm}^{-1}$  (Fig. 7).

In solid deuterium, the corresponding 1350-1290  $\text{cm}^{-1}$  region contains four sharp peaks (Fig. 4). The 1337.2 and 1293.1  $\text{cm}^{-1}$  bands are stronger initially, and they increase on  $\lambda > 290$  photolysis, which almost destroys the 1346.1, 1306.4  $\text{cm}^{-1}$  set. The latter pair dominate after 9.0 K annealing (Fig. 4g). The 1337.2 and 1293.1  $\text{cm}^{-1}$  bands are 12.9 and 14.8  $\text{cm}^{-1}$  above  $\text{AlD}_2$  absorptions in solid argon,<sup>23,25</sup> but 3.2 and 2.9  $\text{cm}^{-1}$  below new neon matrix  $\text{AlD}_2$  bands observed here. Thus, the 1337.2 and 1293.1  $\text{cm}^{-1}$  bands are due to  $\text{AlD}_2$  in solid deuterium.

The  $\text{H}_2 + \text{D}_2$  experiments give several new absorptions (Figs. 2d, 5). In the Al-H region the 1822.7, 1789.4  $\text{cm}^{-1}$  peaks arise from  $\text{AlH}_2$  where 0.8 and 1.6  $\text{cm}^{-1}$  differences are due to the change from pure  $\text{H}_2$ . The new 1807.2  $\text{cm}^{-1}$  band is appropriate for  $\text{AlHD}$  observed 18.4  $\text{cm}^{-1}$  lower at 1788.8  $\text{cm}^{-1}$  in solid argon.<sup>23,25</sup> New 1811.5, 1808.7  $\text{cm}^{-1}$  bands appear to track with the 1834.7, 1832.2, 1822.9  $\text{cm}^{-1}$  set, which exhibits different relative intensities from the analogous pure  $\text{H}_2$  product group. In the Al-D region, new 1337.3 and 1293.3  $\text{cm}^{-1}$  peaks are due to  $\text{AlD}_2$ , and a new 1317.6 band is appropriate for  $\text{AlHD}$  observed 18.3  $\text{cm}^{-1}$  lower at 1299.3  $\text{cm}^{-1}$  in solid argon.<sup>25</sup> A new 1326.3, 1325.1  $\text{cm}^{-1}$  band appears to track with the 1346.0, 1306.8  $\text{cm}^{-1}$  pair.

The pure HD experiment (Figs. 2e, 5) behaved similarly. New bands at 1806.8 and 1315.5  $\text{cm}^{-1}$  due to  $\text{AlHD}$  in pure HD are 0.4 and 2.1  $\text{cm}^{-1}$  different from  $\text{AlHD}$  in the  $\text{H}_2 + \text{D}_2$  sample. New absorptions are observed at 1844.5, 1840.1, 1835.2, 1831.5  $\text{cm}^{-1}$  and at 1341.5, 1331.0  $\text{cm}^{-1}$ .

Lammertsma et al.<sup>51</sup> performed a detailed series of calculations on  $\text{Al}_2\text{H}_4$  structures, and concluded that ionic  $\text{C}_{3v}$  and  $\text{C}_{2v}$  structures are slightly lower in energy than the  $\text{D}_{2d}$   $\text{H}_2\text{AlAlH}_2$  form.

Our B3LYP calculations agree with this conclusion and provide frequencies and infrared intensities that support identification of the  $D_{2d}$  form through the 1838.4, 1835.8, 1825.5  $\text{cm}^{-1}$  band group in solid hydrogen. We have no evidence for the 9.4 and 7.8 kcal/mol lower energy ionic forms. The  $C_{2v}$  structure is predicted to exhibit a very strong  $a_1$  bridge stretching mode at 1198  $\text{cm}^{-1}$  (Table 2). No absorptions occur in this region except for the very strong bridge stretching mode of  $\text{Al}_2\text{H}_2$  observed at 1156.1  $\text{cm}^{-1}$ .

Two strong Al-H stretching modes are predicted at 1899  $\text{cm}^{-1}$  ( $e$ , 544 km/mol) and 1880  $\text{cm}^{-1}$  ( $b_2$ , 409 km/mol) for  $D_{2d}$   $\text{Al}_2\text{H}_4$  (Table 2) where the former is an antisymmetric Al-H<sub>2</sub> stretching mode and the latter is an out-of-phase combination of symmetric Al-H<sub>2</sub> stretching modes on the two  $\text{AlH}_2$  subunits. Furthermore these modes are predicted 37 and 63  $\text{cm}^{-1}$  above the stretching modes of  $\text{AlH}_2$ , and the 1838.4, 1835.8 and 1825.5  $\text{cm}^{-1}$  bands are 15 and 38  $\text{cm}^{-1}$  higher than the  $\text{AlH}_2$  absorptions in solid hydrogen. We also find a correspondence in the H/D isotopic frequency ratios: for  $\text{AlH}_2$ , the H/D frequency ratios are 1.3624 and 1.3826 for the antisymmetric and symmetric modes, respectively, and for the above group 1837.1 (average)/1346.1 = 1.3648 and 1825.5/1306.4 = 1.3974. Scale factors (observed/calculated) using our hydrogen matrix and B3LYP frequencies for  $\text{AlH}_2$  are 0.979 ( $b_2$ ) and 0.984 ( $a_1$ ). Similar scale factors are found for the above group: the split 1838.4, 1835.8  $\text{cm}^{-1}$  band is assigned to the  $e$  mode and the 1825.5  $\text{cm}^{-1}$  band to the  $b_2$  mode of  $\text{Al}_2\text{H}_4$ , and 0.967 ( $e$ ) and 0.971 ( $b_2$ ) scale factors result. All of the above evidence substantiates the present infrared identification of  $D_{2d}$   $\text{Al}_2\text{H}_4$ . The stronger  $e$  mode of  $\text{Al}_2\text{D}_4$  is not split by the  $D_2$  matrix. Our B3LYP calculations predict a strong  $\text{AlH}_2$  bending mode ( $b_2$ , out-of-phase scissors) for  $\text{Al}_2\text{H}_4$  at 758  $\text{cm}^{-1}$ . A broad 747  $\text{cm}^{-1}$  band tracks with the above band group on annealing and photolysis in normal hydrogen and is assigned to the  $b_2$  bending mode of  $\text{Al}_2\text{H}_4$ . In *para*- $\text{H}_2$  this band is sharp at 747.8  $\text{cm}^{-1}$ . Finally, the unique observation of these

bands on deposition of thermal Al atoms with para-H<sub>2</sub> at 2.4 K points to a spontaneous reaction with Al<sub>2</sub> (see Reaction Mechanisms section).

The mixed isotopic experiments provide further support for the identification of Al<sub>2</sub>H<sub>4</sub>. Our B3LYP calculation for AlH<sub>2</sub>AlD<sub>2</sub> predicts two strong absorptions coincident with e modes of the pure isotopic species plus strong bands just 9 and 25 cm<sup>-1</sup> lower in the Al-H and Al-D stretching regions, respectively. The new bands at 1811.5, 1808.7 cm<sup>-1</sup> and 1326.3, 1325.1 cm<sup>-1</sup>, which are 22 and 20 cm<sup>-1</sup> lower than the corresponding bands for the pure isotopic species, are assigned to AlH<sub>2</sub>AlD<sub>2</sub>. Our calculation for AlHDAIH<sub>2</sub>D predicts four new observable bands in these regions, and new bands at 1844.5, 1835.2, 1341.5, and 1331.0 cm<sup>-1</sup> in pure HD are appropriate for the AlHDAIH<sub>2</sub>D isotopic molecule.

Finally, split combination bands are observed for Al<sub>2</sub>H<sub>4</sub> at 3141.4 and for Al<sub>2</sub>D<sub>2</sub> at 2273.6 cm<sup>-1</sup>. These are probably three-mode combination bands.

**Al<sub>2</sub>H<sub>6</sub>.** The seven band DA set has straightforward chemistry. The strongest three bands at 1932.3, 1408.1, and 1268.2 cm<sup>-1</sup> are detected on sample deposition (absorbance 0.001). These bands double on annealing to 6.0 K and double again on λ > 290 nm photolysis while AlH is reduced 90%, AlH<sub>3</sub> increases four-fold, and weaker DA bands join at 1915.1, 835.6, 702.4, and 631.9 cm<sup>-1</sup>. Subsequent λ > 240 nm photolysis increases the DA bands four-fold in concert and the AlH<sub>3</sub> bands two-fold, while the next 6.5 K annealing increases DA bands by 25% at the expense of AlH<sub>3</sub>, and a final λ > 240 nm photolysis increases DA bands by 50% and AlH<sub>3</sub> by 5% (Fig. 1). Thus, AlH<sub>3</sub> is produced on photoexcitation of AlH with excess hydrogen,<sup>23-25</sup> and DA is formed on ultraviolet photolysis along with AlH<sub>3</sub> and on annealing from AlH<sub>3</sub>. The seven DA bands then must be considered for assignment to dialane, Al<sub>2</sub>H<sub>6</sub>. These bands are produced in much greater yield in the softer hydrogen and neon matrices, which allow more diffusion, than the more rigid argon

matrix. Finally, the highest frequency five of these bands are observed in para-H<sub>2</sub> at 1933.5, 1918.6, 1406.1, 1264.3, and 835.2 cm<sup>-1</sup> after ultraviolet photolysis.

Similar experiments were done with pure normal-D<sub>2</sub> and with H<sub>2</sub>+D<sub>2</sub> mixtures. The perdeuterio counterparts for AlD<sub>2</sub>, AlD<sub>3</sub> and all but the weakest DA band are listed in Table 1. The H/D frequency ratios ranging from 1.364 to 1.379 are characteristic of Al-H/Al-D vibrational modes. New information obtained from H<sub>2</sub> + D<sub>2</sub> mixtures includes new absorptions at 1925.5, 1411.7 cm<sup>-1</sup> and at 1036.6 cm<sup>-1</sup> in addition to stronger AlH<sub>2</sub>D, AlHD<sub>2</sub> and AlHD absorptions.<sup>23-26</sup> The new 1925.5 cm<sup>-1</sup> band between pure H<sub>2</sub> product bands at 1932.3 and 1915.1 cm<sup>-1</sup> (Fig. 2d) and the new 1411.7 cm<sup>-1</sup> band between pure D<sub>2</sub> product bands at 1414.9 and 1402.9 cm<sup>-1</sup> indicate that the pure matrix bands are antisymmetric and symmetric AlH<sub>2</sub>(AlD<sub>2</sub>) stretching modes, and their position above AlH<sub>2</sub> points to a terminal AlH<sub>2</sub> subunit. Thus, the intermediate bands are uncoupled Al-H and Al-D stretching modes in a terminal AlHD group. The 1036.6 cm<sup>-1</sup> absorption is slightly higher than 1028.5 cm<sup>-1</sup> pure deuterium counterpart, and this is consistent with an Al-(D)<sub>2</sub>-Al bridging subunit coupled to Al-H motions. The pure HD experiment likewise produced AlH<sub>2</sub>D, AlHD<sub>2</sub> and AlHD plus sharp new absorptions at 1926.5, 1922.6, 1919.4, 1915.7 cm<sup>-1</sup> (Fig. 2f) and at 1416.8, 1415.0, 1412.9, 1406.4 cm<sup>-1</sup>. These bands are clearly due to terminal Al-H and Al-D vibrations in mixed isotopic Al<sub>2</sub>H<sub>x</sub>D<sub>y</sub> (x+y = 6) molecules. Unfortunately, the strongest Al(HD)Al bridge mode is predicted to fall under the strong AlHD<sub>2</sub> absorption.

Table 2 compares previous SCF and CCSD calculated frequencies<sup>7,11</sup> with the present B3LYP harmonic predictions for Al<sub>2</sub>H<sub>6</sub>, which are expected to approach the experimental anharmonic values.<sup>52</sup> Notice that the BPW91 computed Al-H stretching frequencies are closer to the observed values, but the bending frequencies are below the observed values. Liang et al.<sup>7</sup>

also performed similar SCF calculations for  $B_2H_6$  and  $Ga_2H_6$  and showed that the calculated frequencies for the seven strongest infrared active modes, designated 8, 9, 13, 14, 16, 17, 18 in Table 2, are respectively 6.9, 16.4, 5.5, 9.1, 6.8, 11.6, and 8.7% higher than observed values for  $B_2H_6$  and 3.9, 14.7, 4.1, 6.5, 5.0, 10.5, and 8.6% higher than observed for  $Ga_2H_6$ . Their calculated frequencies for  $Al_2H_6$  are likewise 6.7, 19.3, 6.5, 9.8, 7.1, 13.8, and 9.1% higher than our hydrogen matrix DA absorptions. The correlation in these % deviations between calculated and observed  $M_2H_6$  frequencies points to the identification of DA as dialane  $Al_2H_6$ . The 1932 and 1915  $cm^{-1}$  absorptions are antisymmetric  $b_{1u}$  and  $b_{3u}$  terminal Al- $H_2$  stretching modes. The 1408 and 1268  $cm^{-1}$  bands are antisymmetric  $b_{2u}$  and  $b_{3u}$  stretching modes of the bridged Al-( $\mu$ -H) $_2$ -Al subunit. The lower frequency 836, 632, and 702  $cm^{-1}$  absorptions are due to AlH $_2$  wag, rock and bending motions.<sup>7</sup>

A comparison of calculated harmonic (B3LYP) and observed anharmonic (hydrogen matrix) terminal Al-H stretching frequencies (Tables 1, 2, 3) shows that calculated exceed observed values by 40, 29  $cm^{-1}$  for AlH $_2$ , 65  $cm^{-1}$  for AlH $_3$ , 62, 54  $cm^{-1}$  for  $Al_2H_4$ , and 57, 51  $cm^{-1}$  for  $Al_2H_6$ . Part of this discrepancy is due to anharmonicity. The general agreement in these calculated-observed differences underscores the predictive power of quantum chemical calculations and further supports our preparation and identification of  $Al_2H_6$ .

Another means of comparison is the scale factor (observed/calculated frequencies). For our B3LYP calculation, scale factors are 0.971 and 0.974 for the terminal Al- $H_2$  stretching modes, 0.949 and 0.981 for the bridge Al-(H) $_2$ -Al stretching motions, and 0.965, 0.989, and 0.997 for the low-frequency vibrations. Our scale factor for the e stretching mode of AlH $_3$  is 0.967. These typical scale factors for the B3LYP functional<sup>52</sup> further substantiate our identification of dialane from the matrix infrared spectrum. Note that scale factors differ for

different vibrational modes: the potential functions will require anharmonic refinement for better agreement. Confidence in this identification of dialane is built on excellent agreement between observed and calculated frequencies for *seven* fundamental vibrations in three different spectral regions.

Additional agreement is found in the calculated and observed infrared intensities. The strongest band in the infrared spectrum, by about a factor of two, is the antisymmetric  $b_{3u}$  Al-( $\mu$ -H)<sub>2</sub>-Al bridge-bond stretching mode parallel to the Al-Al axis. This 1408 cm<sup>-1</sup> band in our spectrum is broader than the 1268 cm<sup>-1</sup> absorption, which is the antisymmetric  $b_{2u}$  Al-( $\mu$ -H)<sub>2</sub>-Al bridge-bond stretching mode perpendicular to the Al-Al axis. However, the integrated experimental band intensities (Table 2) are in qualitative agreement with the predictions of theory. The terminal Al-H<sub>2</sub>  $b_{1u}$  and  $b_{3u}$  stretching modes are split by interaction with the hydrogen matrix. The higher frequency  $b_{1u}$  mode is predicted (B3LYP) to be three-fold stronger, and the observed relative  $b_{1u}$  and  $b_{3u}$  mode intensities match nicely (Fig. 2c).

Weaker 1362.8 and 1227.8 cm<sup>-1</sup> bands appear along with DA on  $\lambda > 380, 290$  nm photolysis but decrease when DA increases markedly  $\lambda > 240$  nm irradiation (Fig. 1). These bands reappear on 6.5 K annealing while DA slightly increases. The proximity to strong DA bands at 1408.1 and 1268.2 cm<sup>-1</sup> suggests that a perturbed DA species is also formed in the hydrogen matrix.

Alkyl substituents stabilize aluminum hydrides,<sup>53</sup> and the stable compound (CH<sub>3</sub>)<sub>2</sub>Al( $\mu$ -H)<sub>2</sub>Al(CH<sub>3</sub>)<sub>2</sub> has the same dibridged Al( $\mu$ -H)<sub>2</sub>Al subunit as Al<sub>2</sub>H<sub>6</sub>.<sup>54</sup> Recent B3LYP calculations of the Al-H-Al bridge bond length find 1.76 Å, which is almost the same as the present 1.74 Å value for Al<sub>2</sub>H<sub>6</sub>, and association enthalpies computed for (CH<sub>3</sub>)<sub>2</sub>AlH are only 2 kcal/mol less than for AlH<sub>3</sub>.<sup>55</sup> Hence, these aluminum hydride compounds have similar bridge

bonding. Furthermore, calculated (B3LYP) frequencies (1442, 1245  $\text{cm}^{-1}$ )<sup>55</sup> and vapor phase absorptions (1368, 1215  $\text{cm}^{-1}$ )<sup>56</sup> observed for the  $\text{Al}(\text{H})_2\text{Al}$  bridge stretching modes are in excellent agreement for the  $(\text{CH}_3)_2\text{AlH}$  dimer,  $(\text{CH}_3)_2\text{Al}(\mu\text{-H})_2\text{Al}(\text{CH}_3)_2$ , and these diagnostic frequencies are only slightly lower than our corresponding B3LYP (1483, 1292  $\text{cm}^{-1}$ ) and observed (1408, 1268  $\text{cm}^{-1}$ ) values for  $\text{H}_2\text{Al}(\mu\text{-H})_2\text{AlH}_2$ . These comparisons of  $\text{Al}(\text{H}_2)\text{Al}$  bridge stretching frequencies provide further evidence for the present experimental identification of the binary hydride  $\text{H}_2\text{Al}(\mu\text{-H})_2\text{AlH}_2$  molecule.

A final comparison can be made with the infrared active  $\text{M}-(\mu\text{-H})_2\text{-M}$  bridge stretching modes for the three  $\text{M}_2\text{H}_6$  molecules characterized to date,  $\text{M} = \text{B}, \text{Al}, \text{Ga}$ . The  $\nu_{13}$  ( $b_{1u}$ ) modes are 1924, 1268, 1202  $\text{cm}^{-1}$ , respectively, and the  $\nu_{17}$  ( $b_{3u}$ ) modes are 1615, 1408, 1273  $\text{cm}^{-1}$ , respectively.<sup>15,57</sup> The dialane frequencies are intermediate but much closer to digallane than diborane values.

We believe that the infrared spectrum of  $\text{Al}_2\text{H}_6$ , containing seven fundamental absorption bands in terminal  $\text{Al-H}_2$  stretching, bridge  $\text{Al}-(\text{H})_2\text{-Al}$  stretching, and  $\text{Al-H}_2$  bending regions, which are nicely matched by quantum chemical frequency calculations, makes a very strong case for the identification of dialane and its characterization with the diborane bridge-bonding model.

**$\text{Al}_2\text{H}_2$ .** The earlier argon matrix work assigned several bands to  $\text{Al}_2\text{H}_2$  species.<sup>23</sup> The only one of these absorptions observed here is at 1156.1  $\text{cm}^{-1}$  in normal and 1155.0  $\text{cm}^{-1}$  in para- $\text{H}_2$ . More recent calculations show that the  $b_{1u}$  antisymmetric stretching mode of planar dibridged  $\text{Al}_2\text{H}_2$  predicted near 1200  $\text{cm}^{-1}$  is extremely intense, but the corresponding  $b_{2u}$  mode is only 1/20 as strong.<sup>58</sup> Our B3LYP computation found 1187  $\text{cm}^{-1}$  for the  $b_{1u}$  mode. The sharp 844.1  $\text{cm}^{-1}$  band does not track on  $\lambda > 530$  nm photolysis, which destroys the 1156.1  $\text{cm}^{-1}$  band

in favor of  $\text{Al}_2\text{H}_6$ . Hence, the  $1156.1\text{ cm}^{-1}$  band is assigned to the most stable  $\text{Al}_2\text{H}_2$  isomer, dibridged  $\text{Al}-(\mu\text{-H})_2\text{-Al}$ , which is the only form observed in solid hydrogen.

$\text{AlH}_4^-$ ,  $\text{AlD}_4^-$  and  $\text{AlD}_2^-$ . The  $1638.1\text{ cm}^{-1}$  absorption appears above a  $1609.3\text{ cm}^{-1}$  photolysis product in the argon/Al/ $\text{H}_2$  system, which has been conclusively identified as  $\text{AlH}_4^-$  isolated in solid argon.<sup>48</sup> The  $1638.1\text{ cm}^{-1}$  band increases on  $\lambda > 380, 290\text{ nm}$  photolysis but decreases on  $\lambda > 240\text{ nm}$  irradiation (Fig. 1). The  $1638.1\text{ cm}^{-1}$  band decreases in yield relative to the  $\text{AlH}_3$  band with increasing laser energy. In pure deuterium the  $1183.2\text{ cm}^{-1}$  counterpart is weak, but a  $1050.0, 1043.0\text{ cm}^{-1}$  doublet gives way on  $\lambda > 290\text{ nm}$  photolysis and doubles the  $1183.2\text{ cm}^{-1}$  absorption, but  $\lambda > 240\text{ nm}$  irradiation virtually destroys this feature. Pure HD gives new counterpart absorptions at  $1658.1$  and  $1193.9\text{ cm}^{-1}$  for  $\text{AlH}_2\text{D}_2^-$ , which supports assignment of the  $1638.1\text{ cm}^{-1}$  band to  $\text{AlH}_4^-$  in solid hydrogen. This is in agreement with the present and previous<sup>48</sup> DFT calculations for the  $\nu_3(t_2)$  fundamental of tetrahedral  $\text{AlH}_4^-$ .

The photosensitive  $1050.0, 1043.0\text{ cm}^{-1}$  band pair in solid  $\text{D}_2$  is extremely close to our B3LYP prediction of  $1058.4(a_1)$  and  $1056.9\text{ cm}^{-1}(b_2)$  modes for  $\text{AlD}_2^-$ . Since our B3LYP calculation found  $1190.2\text{ cm}^{-1}$  for  $\nu_3(t_2)$  of  $\text{AlD}_4^-$ , only  $7.0\text{ cm}^{-1}$  above the observed value in solid  $\text{D}_2$ , the  $1050.0$  and  $1043.0\text{ cm}^{-1}$  bands are assigned to  $\nu_1(a_1)$  and  $\nu_3(b_2)$  of  $\text{AlD}_2^-$ . This observation means that  $\text{AlD}_2^-$  is stable in solid  $\text{D}_2$ , but  $\lambda > 290\text{ nm}$  radiation initiates reaction with  $\text{D}_2$  to form  $\text{AlD}_4^-$ . However, the corresponding  $\text{AlH}_2^-$  species was not observed in solid  $\text{H}_2$ . This suggests that any  $\text{AlH}_2^-$  formed reacts straightaway with  $\text{H}_2$  to form  $\text{AlH}_4^-$ , which is observed at  $1638.1\text{ cm}^{-1}$  in solid  $\text{H}_2$ .

$(\text{AlH}_3)_n$ . When the hydrogen matrix samples are annealed to  $6.8\text{ K}$ ,  $\text{H}_2$  evaporates, molecular aluminum hydrides diffuse, aggregate and their absorptions decrease, and broad

absorptions appear at  $1720 \pm 20$  and  $720 \pm 20$   $\text{cm}^{-1}$  (Fig. 3 a,b,c). These broad bands remain on the CsI window with decreasing absorbance until room temperature is reached. The deuterium matrix samples evaporate  $\text{D}_2$  at about 10 K and aluminum deuterides produce a broad  $1260 \pm 20$   $\text{cm}^{-1}$  absorption (Fig. 3d,e), which remains on the CsI window. The ratio  $1720/1260 = 1.365$  demonstrates that these bands are due to Al-H/Al-D vibrations. The aluminum/ $\text{H}_2/\text{D}_2$  samples produce similar broad bands after evaporation of the matrix that are shifted slightly to  $1740 \pm 20$ ,  $1280 \pm 20$  and  $710 \pm 20$   $\text{cm}^{-1}$  (Fig. 3f).

The spectrum of pure solid  $(\text{AlH}_3)_n$  gives strong broad bands at 1760 and 680  $\text{cm}^{-1}$  and solid  $(\text{AlH}_3)_n$  in nujol reveals a very strong, broad 1592  $\text{cm}^{-1}$  band, and solid  $(\text{AlD}_3)_n$  gives a corresponding 1163  $\text{cm}^{-1}$  band.<sup>59,60</sup> The present broad absorptions 1720 and 1260  $\text{cm}^{-1}$  are therefore due to solid  $(\text{AlH}_3)_n$  and  $(\text{AlD}_3)_n$  on the CsI salt window. Since the Al-H bond is polar,<sup>16</sup> the solid  $(\text{AlH}_3)_n$  network<sup>5</sup> may align and bind electrostatically to the ionic CsI lattice surface. The 100  $\text{cm}^{-1}$  redshift in nujol is due to interaction with this host medium.

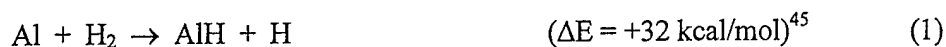
Our broad 720  $\text{cm}^{-1}$  absorption corresponds to the 680  $\text{cm}^{-1}$  solid band.<sup>59</sup> These bands are higher than our 632  $\text{cm}^{-1}$   $\text{Al}_2\text{H}_6$  absorption, which probably involves bending of the Al-H-Al bridge bonds. A very weak  $520 \pm 20$   $\text{cm}^{-1}$  absorption on our cold window (Fig. 3 e) may be the deuterium counterpart of the 508  $\text{cm}^{-1}$  nujol band.

The crystal structure for solid  $(\text{AlH}_3)_n$  shows six-coordinate aluminum with all hydrogen atoms in bridge-bonding arrangements between aluminum atoms.<sup>5</sup> The average Al-H distance is 1.72 Å. It is interesting to note that the solid Al-H distance is intermediate between the 1.74 Å bridge and 1.58 Å terminal Al-H distances calculated here for  $\text{Al}_2\text{H}_6$  and that the solid frequency of 1720  $\text{cm}^{-1}$  is likewise intermediate between the terminal (1932, 1915  $\text{cm}^{-1}$ ) and bridged (1408, 1268  $\text{cm}^{-1}$ )  $\text{Al}_2\text{H}_6$  values observed here.

Evaporation of the H<sub>2</sub>, D<sub>2</sub> matrix from mixed H, D aluminum hydride samples gave similar broad bands slightly blue shifted. This shows a slight stretch-stretch interaction for Al-H-Al bonds in the solid state and suggests that the symmetric stretching modes in (AlH<sub>3</sub>)<sub>n</sub> are higher than the observed antisymmetric stretching modes.

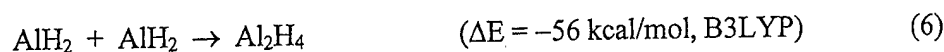
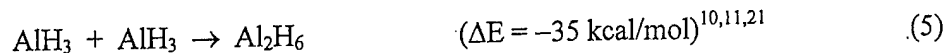
Finally, it is interesting to observe that these reactions take Al and H<sub>2</sub> to the molecular aluminum hydrides AlH<sub>3</sub> and Al<sub>2</sub>H<sub>6</sub>, which aggregate in the end to form (AlH<sub>3</sub>)<sub>n</sub> solids. Thus, we have explored aluminum-hydrogen chemistry from the microscopic beginning to the macroscopic end using the matrix isolation technique.

**Reaction mechanisms.** The reaction of Al and H<sub>2</sub> must be activated by photolysis<sup>24,25,61</sup> or by excess energy (kinetic or photon) from the ablation process.<sup>32,62</sup>

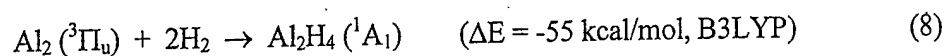
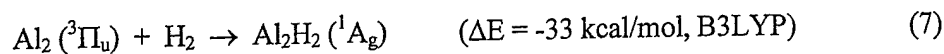


The growth of AlH<sub>2</sub> on annealing, Fig. 1f, requires that H atoms diffuse and react with AlH, reaction 3. The production of H atoms in laser ablation/solid hydrogen experiments has been documented through the observation of HO<sub>2</sub> radical.<sup>49</sup> Photoexcitation of AlH at 3.0 eV (Fig. 1c) in the presence of hydrogen leads to the formation of AlH<sub>3</sub>, reaction 4. Then Al<sub>2</sub>H<sub>6</sub> is formed by the dimerization of AlH<sub>3</sub>, reaction 5. Although a small growth of Al<sub>2</sub>H<sub>6</sub> absorptions is found on annealing the solid hydrogen samples, more growth is observed on λ > 240 nm irradiation when the AlH<sub>3</sub> monomer yield increases markedly. A strong satellite absorption at 1370.5 cm<sup>-1</sup> on the 1378.7 cm<sup>-1</sup> AlD<sub>3</sub> absorption may be due to unreacted (AlD<sub>3</sub>)<sub>2</sub> dimers. The absence of a similar satellite absorption for AlH<sub>3</sub> suggests a small activation energy for reaction 5 in the case of AlD<sub>3</sub>.

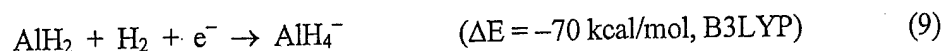
The straightforward formation of  $D_{2d}$   $Al_2H_4$  involves the exothermic dimerization of  $AlH_2$ , reaction 6. We find no evidence for the ionic  $Al_2H_4$  isomers.<sup>51</sup> It is important to note that  $Al_2H_4$  is formed on sample deposition when the yield of  $AlH_2$  is large and that  $Al_2H_6$  is favored after ultraviolet photolysis when the yield of  $AlH_3$  is high.

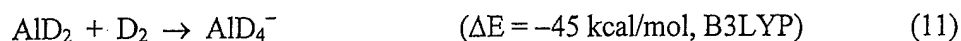
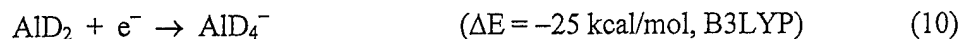


A unique synthesis of  $Al_2H_4$  is observed from the recombination of thermal Al atoms during deposition in para- $H_2$ ; see especially Fig 7a where  $Al_2H_4$  dominates over the small amount of  $AlH$  produced during deposition by the ultraviolet spectroscopic diagnostic. Apparently the exothermic ( $30.0 \pm 1.4$  kcal/mol)<sup>63</sup> dimerization of Al atoms to form  $^3\Pi_u$  ground-state  $Al_2$ <sup>63,64</sup> is sufficient to activate one or two dihydrogen molecules to form  $Al_2H_2$  and  $Al_2H_4$ , reactions 7 and 8. Hence variable amounts of  $Al_2H_2$  and  $Al_2H_4$  are observed from these reactions on thermal Al deposition with para- $H_2$ . Even though the  $Al_2$  reaction with  $3H_2$  is even more exothermic (-87 kcal/mol, B3LYP), inserting  $(\mu-H)_2$  into the Al-Al bond in  $Al_2H_4$  must require substantial activation energy. However, dibridged  $Al-(\mu-H)_2-Al$  can be activated by  $\lambda > 530$  nm photolysis to form  $Al_2H_6$  in solid hydrogen.



The stable  $AlH_4^-$  anion is formed by capture of electrons from the ablation process. We note that no  $AlH_4^-$  counterpart is observed with thermal Al atoms in para- $H_2$ . The electron affinity of  $AlD_2$  is estimated as 25 kcal/mol (B3LYP). In solid deuterium experiments,  $AlD_2^-$  is trapped and  $\lambda > 290$  nm photoexcitation leads directly to  $AlD_4^-$ .





The final reaction, the formation of solid aluminum hydride, happens on evaporation of the hydrogen matrix to allow association of molecular aluminum hydrides. This solid  $(\text{AlH}_3)_n$  is identified by agreement of broad infrared absorption bands with spectra of the pure solid.<sup>59</sup> Reaction 12 is estimated to be exothermic by 40 kcal *per mole of AlH<sub>3</sub>*, which contributes to the stability of the solid.<sup>16</sup> It appears, then, that the failure to isolate  $\text{Al}_2\text{H}_6$  is due to its polymerization into the more stable network solid, which is observed in these hydrogen matrix experiments.



The successful synthesis and characterization of  $\text{Al}_2\text{H}_6$  is made possible by special chemical and physical properties of the pure hydrogen matrix. The "high" hydrogen concentration ensures the formation of a large yield of  $\text{AlH}_3$  and the soft nature of solid hydrogen allows diffusion and dimerization of  $\text{AlH}_3$ . When the temperature of the solid hydrogen sample approaches 7 K,  $\text{H}_2$  evaporates, the diffusion and reaction of trapped aluminum hydride molecules is rapid, and solid  $(\text{AlH}_3)_n$  is formed.

## Conclusions

The reaction of laser-ablated Al atoms and normal- $\text{H}_2$  during codeposition at 3.5 K forms  $\text{AlH}$ ,  $\text{AlH}_2$ , and  $\text{AlH}_3$  based on infrared spectra, and the results of isotopic substitution ( $\text{D}_2$ ,  $\text{H}_2 + \text{D}_2$  mixtures, HD). Four new bands are assigned to  $\text{Al}_2\text{H}_4$  with the  $\text{D}_{2d}$  structure. Ultraviolet photolysis markedly increases the yield of  $\text{AlH}_3$  and seven new absorptions for  $\text{Al}_2\text{H}_6$  in the infrared spectrum of the solid hydrogen sample. Complementary results are found using thermal Al atoms and para- $\text{H}_2$ . These seven vibrational frequencies are accurately predicted by quantum chemical calculations for dibridged  $\text{Al}_2\text{H}_6$ , which is isostructural with diborane. Annealing these

samples to remove the H<sub>2</sub> matrix decreases the sharp AlH<sub>3</sub> and Al<sub>2</sub>H<sub>6</sub> absorptions and produces broad 1720±20 and 720±20 cm<sup>-1</sup> bands, which are due to solid (AlH<sub>3</sub>)<sub>n</sub> on the CsI window. Small matrix shifts are observed between normal hydrogen (3/4 ortho-H<sub>2</sub>, 1/4 para-H<sub>2</sub>)<sup>66</sup> and para-H<sub>2</sub>. The novel formation of Al<sub>2</sub>H<sub>4</sub> during deposition in para-H<sub>2</sub> from the exothermic combination of Al atoms assists identification of this novel molecule. Although many volatile binary boron hydride compounds are known, binary aluminum hydride chemistry is limited to the polymeric (AlH<sub>3</sub>)<sub>n</sub> solid. Our experimental characterization of the dibridged Al<sub>2</sub>H<sub>6</sub> molecule provides an important link between the chemistries of boron and aluminum.

**Acknowledgment.** We thank G. V. Chertihin and P. F. Souter for work on earlier experiments and NSF Grant CHE00-78836 for financial support.

#### References

- (1) Stock, A., *Hydrides of Boron and Silicon*, Cornell University Press, Ithaca, 1933.
- (2) Lipscomb, W. N. *Boron Hydrides*, W. A. Benjamin, New York, 1963.
- (3) Greenwood, N. N. *Chem. Soc. Rev.* **1992**, *21*, 49.
- (4) Cotton, F. A.; Wilkinson, G.; Murillo, C. A.; Bochmann, M. *Advanced Inorganic Chemistry*, Wiley: New York, ed. 6, 1999.
- (5) Turley, J. W.; Rinn, H. W. *Inorg. Chem.* **1969**, *8*, 18.
- (6) Brower, F. M.; Matzek, N. E.; Reigler, P. F.; Rinn, H. W.; Roberts, C. B.; Schmidt, D. L.; Snover, J. A.; Terada, K. *J. Am. Chem. Soc.* **1976**, *98*, 2450.
- (7) Liang, C.; Davy, R. D.; Schaeffer, III, H. F. *Chem. Phys. Lett.* **1989**, *159*, 393.
- (8) Lammertsma, K.; Leszczynski, J. *J. Phys. Chem.* **1990**, *94*, 2806.
- (9) Bock, C. W.; Trachtman, M.; Murphy, C.; Muschert, B.; Mains, G. J. *J. Phys. Chem.* **1991**, *95*, 2339.
- (10) Duke, B. J.; Liang, C.; Schaefer, H. F., III. *J. Am. Chem. Soc.* **1991**, *113*, 2884.
- (11) Shen, M.; Schaefer, III, H. F. *J. Chem. Phys.* **1992**, *96*, 2868.

- (12) Barone, V.; Orlandini, L.; Adamo, C. *J. Phys. Chem.* **1994**, *98*, 13185.
- (13) Magers, D. H.; Hood, R. B.; Leszczynski, J. *Int. J. Quant. Chem. Symp.* **1994**, *28*, 579.
- (14) Downs, A. J.; Goode, M. J.; Pulham, C. R. *J. Am. Chem. Soc.* **1989**, *111*, 1936.
- (15) Pulham, C. R.; Downs, A. J.; Goode, M. J.; Rankin, D. W. H.; Robertson, H. E. *J. Am. Chem. Soc.* **1991**, *113*, 5149.
- (16) Downs, A. J.; Pulham, C. R. *Chem. Soc. Rev.* **1994**, *1994*, 175.
- (17) Siegel, B. *J. Am. Chem. Soc.* **1960**, *82*, 1535.
- (18) Breisacher, P.; Siegel, B. *J. Am. Chem. Soc.* **1964**, *86*, 5053.
- (19) Hara, M.; Domen, K.; Onishi, T.; Nozoye, H. *J. Phys. Chem.* **1991**, *95*, 6.
- (20) Rao, B. K.; Jena, P.; Burkart, S.; Ganteför, G.; Seifert, G. *Phys. Rev. Letts.* **2001**, *86*, 692.
- (21) Kohdoh, H.; Hara, M.; Domen, K.; Nozoye, H. *Surf. Sci.* **1993**, *287-288*, 74.
- (22) Zhu, Y. F.; Shehadeh, R.; Grant, E. R. *J. Chem. Phys.* **1992**, *97*, 883.
- (23) Chertihin, G. V.; Andrews, L. *J. Phys. Chem.* **1993**, *97*, 10295.
- (24) Kurth, F. A.; Eberlein, R. A.; Schnöckel, H.; Downs, A. J.; Pulham, C. R. *J. Chem. Soc. Chem. Comm.* **1993**, 1302.
- (25) Pullumbi, P.; Mijoule, C.; Manceron, L.; Bouteiller, Y. *Chem. Phys.* **1994**, *185*, 13.
- (26) Pullumbi, P.; Bouteiller, Y.; Manceron, L.; Mijoule, C. *Chem. Phys.* **1994**, *185*, 25.
- (27) Weltner, W., Jr.; Van Zee, R. J.; Li, S. *J. Phys. Chem.* **1995**, *99*, 6277.
- (28) Fajardo, M.E., Tam, S., Thompson, T.L., Cordonnier, M.E. *Chem. Phys.* **1994**, *189*, 351.
- (29) Wang, X.; Andrews, L. *J. Phys. Chem. A* **2003**, *107*, ASAP (Cr + H<sub>2</sub>).
- (30) Andrews, L.; Wang, X. *J. Am. Chem. Soc.* **2002**, *124*, 7280.
- (31) Tam, S.; Macler, M.; DeRose, M. E.; Fajardo, M. E. *J. Chem. Phys.* **2000**, *113*, 9067.
- (32) Andrews, L.; Burkholder, T. R.; Yustein, J. T. *J. Phys. Chem.* **1992**, *96*, 10182.
- (33) Andrews, L.; Citra, A. *Chem. Rev.* **2002**, *102*, 885.

- (34) Tam, S.; Fajardo, M. *Rev. Sci. Inst.* **1999**, *70*, 1926.
- (35) Fajardo, M.E., Tam, S. *J. Chem. Phys.* **1998**, *108*, 4237.
- (36) Tam, S., Fajardo, M.E. *Appl. Spectrosc.*, **2001**, *55*, 1634.
- (37) Frisch, M. J.; Trucks, G. W.; Schlegel, H. B.; Scuseria, G. E.; Robb, M. A.; Cheeseman, J. R.; Zakrzewski, V. G.; Montgomery, J. A., Jr.; Stratmann, R. E.; Burant, J. C.; Dapprich, S.; Millam, J. M.; Daniels, A. D.; Kudin, K. N.; Strain, M. C.; Farkas, O.; Tomasi, J.; Barone, V.; Cossi, M.; Cammi, R.; Mennucci, B.; Pomelli, C.; Adamo, C.; Clifford, S.; Ochterski, J.; Petersson, G. A.; Ayala, P. Y.; Cui, Q.; Morokuma, K.; Malick, D. K.; Rabuck, A. D.; Raghavachari, K.; Foresman, J. B.; Cioslowski, J.; Ortiz, J. V.; Stefanov, B. B.; Liu, G.; Liashenko, A.; Piskorz, P.; Komaromi, I.; Gomperts, R.; Martin, R. L.; Fox, D. J.; Keith, T.; Al-Laham, M. A.; Peng, C. Y.; Nanayakkara, A.; Gonzalez, C.; Challacombe, M.; Gill, P. M. W.; Johnson, B.; Chen, W.; Wong, M. W.; Andres, J. L.; Gonzalez, C.; Head-Gordon, M.; Replogle, E. S.; Pople, J. A. *Gaussian 98*, Revision A.6, Gaussian, Inc., Pittsburgh PA, 1998.
- (38) Krishnan, R.; Binkley, J. S.; Seeger, R.; Pople, J. A. *J. Chem. Phys.* **1980**, *72*, 650.
- (39) Frisch, M.J.; Pople, J.A.; Binkley, J. S. *J. Chem. Phys.* **1984**, *80*, 3265.
- (40) Becke, A. D. *Phys. Rev. A* **1988**, *38*, 3098.
- (41) Perdew J. P., *Phys. Rev. B* **1983**, *33*, 8822.
- (42) Perdew, J.P.; Wang, Y. *Phys. Rev. B* **1992**, *45*, 13244.
- (43) Becke, A.D. *J. Chem. Phys.* **1993**, *98*, 5648.
- (44) Stevens, P. J.; Devlin, F. J.; Chablowski, C. F.; Frisch, M. J. *J. Phys. Chem.* **1994**, *98*, 11623.
- (45) Huber, K. P.; Herzberg, G. *Constants of Diatomic Molecules*, Van Nostrand, Princeton, 1979.
- (46) Deutsch, J. L.; Neil, W. S.; Ramsay, D. A. *J. Mol. Spectrosc.* **1987**, *125*, 115.
- (47) Wright, R. B.; Bates, J. K.; Gruen, D. M. *Inorg. Chem.* **1978**, *17*, 2275.
- (48) Pullumbi, P.; Bouteiller, Y.; Manceron, L. *Chem. Phys.* **1994**, *101*, 3610.
- (49) Wang, X.; Andrews, L.; Chertihin, G. V.; Souter, P. F. *J. Phys. Chem. A* **2002**, *106*, 6302.
- (50) Fajardo, M.E. *unpublished*.

- (51) Lammertsma, K.; Güner, O. F.; Drewes, R. M., Reed, A. E.; Schleyer, P. v. R. *Inorg. Chem.* **1989**, *28*, 313.
- (52) Scott, A. P.; Radom, L. *J. Phys. Chem.* **1996**, *100*, 16502.
- (53) Schulz, S. *Coord. Chem. Rev.* **2001**, *215*, 1.
- (54) Almenningen, A.; Anderson, G. A.; Forgaard, F. R.; Haaland, A. *Acta Chem. Scand.* **1972**, *26*, 2315.
- (55) Willis, B. G.; Jensen, K. F. *J. Phys. Chem. A* **1998**, *102*, 2613.
- (56) Grady, A. S.; Puntambekar, S. G.; Russell, D. K. *Spectrochim. Acta* **1991**, *47A*, 47.
- (57) Duncan, J. L. *J. Mol. Spectrosc.* **1985**, *113*, 63.
- (58) Stephens, J. C.; Bolton, E. E.; Schaefer, H. F., III; Andrews, L. *J. Chem. Phys.* **1997**, *107*, 119.
- (59) Matzek, W. E.; Musinski, D. F., *U. S. Patent* 3, 883, 644 (1975); *Chem. Abstr.* **1975**, *83*, 45418.
- (60) Roszinski, W.; Dantel, R.; Zeil, W. *Z. Physik. Chem. (Frankfort)* **1963**, *36*, 26.
- (61) Parnis, J. M.; Ozin, G. A. *J. Phys. Chem.* **1989**, *93*, 1215.
- (62) Kang, H.; Beauchamp, J. L. *J. Phys. Chem.* **1985**, *89*, 3364.
- (63) Fu, Z.; Lemire, G. W.; Bishea, G. A.; Morse, M. D. *J. Chem. Phys.* **1990**, *93*, 8420.
- (64) Cai, M. F.; Dzugan, T. P.; Bondybey, V. E. *Chem. Phys. Lett.* **1989**, *155*, 430.
- (65) Gush, H. P.; Hare, W. F. J.; Allin, E. F.; Welsh, H. L. *Can. J. Phys.* **1960**, *38*, 176.
- (66) Silvera, I. F. *Rev. Mod. Phys.* **1980**, *52*, 393.

**Table 1.** Infrared absorptions ( $\text{cm}^{-1}$ ) observed from codeposition of laser-ablated Al atoms and with Ne/H<sub>2</sub>, pure normal H<sub>2</sub>, and Ar/H<sub>2</sub> at 3.5 K.

| Ne/H <sub>2</sub> | Ne/D <sub>2</sub> | H <sub>2</sub> | D <sub>2</sub> | Ar/H <sub>2</sub> | Identification  |
|-------------------|-------------------|----------------|----------------|-------------------|---|
|                   |                   | 4109           | 2958           |                   | (H <sub>2</sub> )AlH                                  |
|                   |                   | 4061.6         | 2919.6         |                   | (H <sub>2</sub> )AlH <sub>3</sub>                     |
|                   |                   | 3141.4         | 2273.6         |                   | Al <sub>2</sub> H <sub>4</sub> combo                  |
|                   |                   | 3138.6         | 2270.8         |                   | Al <sub>2</sub> H <sub>4</sub> combo                  |
| 1931.4            | 1415.8            | 1932.3         | 1414.9         | 1922.2            | DA  |
|                   |                   | 1927.2         | 1413.4         | 1911.4            | DA site   |
| 1923.1            | 1396.1            | 1915.1         | 1402.9         | 1905.7            | DA  |
|                   |                   | 1909.1         | 1401.0         | 1897.3            | DA site   |
| 1889.1            | 1381.3            | 1883.7         | 1378.7         | 1882.6            | AlH <sub>3</sub> (v <sub>3</sub> , e)                 |
| 1840.8            | 1345.8            | 1838.4         | 1346.1         | 1822.8            | Al <sub>2</sub> H <sub>4</sub>                        |
|                   |                   | 1835.8         |                |                   | Al <sub>2</sub> H <sub>4</sub>                        |
|                   |                   | 1825.5         | 1306.4         | 1812.0            | Al <sub>2</sub> H <sub>4</sub>                        |
| 1828.6            | 1340.4            | 1821.9         | 1337.2         | 1806.0            | AlH <sub>2</sub> (v <sub>3</sub> , b <sub>2</sub> )   |
| 1794.7            | 1296.0            | 1787.8         | 1293.1         | 1769.6            | AlH <sub>2</sub> (v <sub>1</sub> , a <sub>1</sub> )   |
|                   |                   | 1751.2         | 1272.4         | 1743.7            |   |
| 1627.8            | 1186.9            | 1638.1         | 1183.2         | 1608.8            | AlH <sub>4</sub> <sup>-</sup>                         |
|                   |                   | 1610.7         | 1169.6         |                   | AlH site  |
| 1610.8            | 1171.0            | 1598.7         | 1163.1         | 1590.7            | AlH   |
|                   |                   | 1504.9         |                |                   | AlH <sub>4</sub> <sup>-</sup>                         |
|                   |                   |                | 1050.0         |                   | AlD <sub>2</sub> <sup>-</sup>                         |
|                   |                   |                | 1043.0         |                   | AlD <sub>2</sub> <sup>-</sup>                         |
| 1404.7            | 1032.5            | 1408.1         | 1028.5         | 1388.0            | DA  |
| 1260.2            | 925.3             | 1268.2         | 919.7          | 1243.4            | DA  |
|                   |                   | 1156.1         |                |                   | Al <sub>2</sub> H <sub>2</sub>                        |
|                   |                   | 844.1          |                |                   |   |
| 835.0             | 607.3             | 835.6          | 607.5          |                   | DA  |
| 782.9             | 562.9             | 777.9          | 561.8          | 783.5             | AlH <sub>3</sub> (v <sub>4</sub> , e)                 |
| 770.7             |                   | 770.5          | 568.2          | 766               | AlH <sub>4</sub> <sup>-</sup>                         |
|                   |                   | 770.5          | 560.3          | 766               | AlH <sub>2</sub>                                      |
|                   |                   | 747            | 563            |                   | Al <sub>2</sub> H <sub>4</sub>                        |
| 712.2             | 523.2             | 711.3          | 522.0          | 697.7             | AlH <sub>3</sub> (v <sub>2</sub> , a <sub>2</sub> '') |
| 703.1             | 511.6             | 702.4          | 510.6          |                   | DA  |
| 630.2             |                   | 631.9          |                |                   | DA  |

**Table 2.** Calculated (B2LYP/6-311++G\*\*) Structures and Frequencies for Aluminum Hydride

Molecules

| molecule  | lengths, Å, angles                           | frequencies, cm <sup>-1</sup> (intensities, km/mol)  |
|---|--|--|
| AlH ( <sup>1</sup> Σ <sup>+</sup> )   | 1.666  | 1642.2 (732)   |
| AlH <sub>2</sub> ( <sup>2</sup> A <sub>1</sub> )<br>(C <sub>2v</sub> )  | 1.603, 118.1°                                | 1861.9 (b <sub>2</sub> , 346), 1817.0 (a <sub>1</sub> , 91), 768.9 (a <sub>1</sub> , 278)  |
| AlH <sub>3</sub> ( <sup>1</sup> A <sub>1</sub> )<br>(D <sub>3h</sub> )  | 1.584  | 1948.7 (e, 272×2), 1939.1 (a <sub>1</sub> , 0), 799.4 (e, 233×2),<br>713.1 (a <sub>2</sub> '', 380)  |
| AlH <sub>2</sub> <sup>-</sup> ( <sup>1</sup> A <sub>1</sub> ) <sup>a</sup><br>(C <sub>2v</sub> )              | 1.699, 94.6°                                 | 1474.4 (a <sub>1</sub> , 1473), 1466.0 (b <sub>2</sub> , 1466.0),<br>808.7 (a <sub>1</sub> , 383)  |
| AlH <sub>2</sub> <sup>+</sup> ( <sup>1</sup> Σ <sub>g</sub> <sup>+</sup> ) <sup>b</sup><br>(D <sub>∞h</sub> ) | 1.551  | 2133.5 (σ <sub>u</sub> , 0.4), 2034.9 (σ <sub>g</sub> , 0), 567.5 (π <sub>u</sub> , 130×2)   |
| AlH <sub>4</sub> <sup>-</sup> ( <sup>1</sup> A <sub>1</sub> ) <sup>c</sup><br>(T <sub>d</sub> )               | 1.644  | 1735.4 (a <sub>1</sub> , 0), 1648.5 (t <sub>2</sub> , 713×3), 783.2 (t <sub>2</sub> , 535×3),<br>763.0 (e, 0×2)  |
| Al <sub>2</sub> H <sub>2</sub> ( <sup>1</sup> A <sub>g</sub> )<br>(D <sub>2h</sub> )                          | 1.831, 2.976                                 | 1359 (a <sub>g</sub> , 0), 1187 (b <sub>1u</sub> , 2064), 1070 (b <sub>3g</sub> , 0)<br>966 (b <sub>2u</sub> , 118), 315 (a <sub>g</sub> , 0), 234 (b <sub>3u</sub> , 157)   |
| HAL(H) <sub>3</sub> Al ( <sup>1</sup> A <sub>1</sub> ) <sup>d</sup><br>(C <sub>3v</sub> )                     | 1.578, 1.676, 1.976,<br>128.0°, 86.0°, 70.7° | 1953 (a <sub>1</sub> , 340), 1694 (a <sub>1</sub> , 75), 1574 (e, 43×2),<br>936 (a <sub>1</sub> , 851), 895 (e, 46×2), 821 (e, 323×2),<br>411 (a <sub>1</sub> , 72), 384 (e, 0×2)  |
| H <sub>2</sub> Al(H) <sub>2</sub> Al ( <sup>1</sup> A <sub>1</sub> )<br>(C <sub>2v</sub> )                    | 1.585, 1.715, 1.864,<br>125.5°, 81.7°, 74.0° | 1934 (b <sub>1</sub> , 24), 1921 (a <sub>1</sub> , 127), 1579 (a <sub>1</sub> , 461),<br>1357 (b <sub>2</sub> , 3), 1198 (a <sub>1</sub> , 1065), 1085 (b <sub>2</sub> , 395),<br>820 (b <sub>1</sub> , 132), 730 (a <sub>1</sub> , 341), 672 (a <sub>2</sub> , 0),<br>513 (b <sub>2</sub> , 29), 332 (a <sub>1</sub> , 40), 127 (b <sub>1</sub> , 19) |
| H <sub>2</sub> AlAlH <sub>2</sub> ( <sup>1</sup> A <sub>1</sub> )<br>(D <sub>2d</sub> )                       | 1.594, 2.592, 115.9°                         | 1901 (a <sub>1</sub> , 0), 1899 (e, 272×2), 1880 (b <sub>2</sub> , 409),<br>819 (a <sub>1</sub> , 0), 758 (b <sub>2</sub> , 719), 549 (e, 75×2),<br>340 (a <sub>1</sub> , 0), 306 (e, 73×2), 149 (b <sub>1</sub> , 0)  |

<sup>a</sup>AlH<sub>2</sub><sup>-</sup> is 25.3 kcal/mol lower energy than AlH<sub>2</sub>. <sup>b</sup>AlH<sub>2</sub><sup>+</sup> is 166 kcal/mol higher energy than AlH<sub>2</sub>. <sup>c</sup>AlH<sub>4</sub><sup>-</sup> is 69.9 kcal/mol lower energy than AlH<sub>2</sub> + H<sub>2</sub>. <sup>d</sup>C<sub>3v</sub> structure is global minimum: C<sub>2v</sub> structure is 1.6 kcal/mol higher, and D<sub>2d</sub> structure is 9.4 kcal/mol higher.

**Table 3.** Comparison of calculated and observed infrared active frequencies ( $\text{cm}^{-1}$ ) for dibridged

$\text{Al}_2\text{H}_6$ .

| sym             | mode <sup>a</sup> | SCF/TZP <sup>b</sup> | CCSD/DZP <sup>c</sup> | B3LYP <sup>d</sup> | BPW91 <sup>d</sup> | observed <sup>e</sup> |
|-----------------|-------------------|----------------------|-----------------------|--------------------|--------------------|-----------------------|
| b <sub>1u</sub> | 8                 | 2062 (518)           | 2047 (344)            | 1989 (419)         | 1934 (379)         | 1932 (0.069)          |
|                 | 9                 | 977 (393)            | 954 (317)             | 866 (244)          | 808 (199)          | 836 (0.037)           |
|                 | 10                | 249 (18)             | 235 (15)              | 223 (13)           | 205 (10)           | -                     |
| b <sub>2u</sub> | 13                | 1350 (544)           | 1368 (463)            | 1292 (352)         | 1275 (291)         | 1268 (0.053)          |
|                 | 14                | 694 (353)            | 664 (328)             | 634 (263)          | 607 (230)          | 632 (0.039)           |
| b <sub>3u</sub> | 16                | 2051 (101)           | 2024 (88)             | 1966 (126)         | 1908 (130)         | 1915 (0.023)          |
|                 | 17                | 1603 (1399)          | 1589 (1162)           | 1483 (1096)        | 1431 (968)         | 1408 (0.128)          |
|                 | 18                | 766 (890)            | 744 (684)             | 712 (648)          | 683 (575)          | 702 (0.048)           |

<sup>a</sup>Symmetry ( $D_{2h}$  point group) and mode description from ref. 7. <sup>b</sup>Ref. 7, calculated intensities ( $\text{km/mol}$ ) in parentheses. <sup>c</sup>Ref. 11. <sup>d</sup>This work, 6-311++G\*\* basis set. <sup>e</sup>In solid hydrogen, integrated intensities at maximum yield in parentheses.

## Figure Captions

**Figure 1.** Infrared spectra in the 2000-1100 and 900-600  $\text{cm}^{-1}$  regions for laser-ablated Al co-deposited with normal hydrogen at 3.5 K. (a) Spectrum of sample deposited for 25 min, (b) after annealing to 6.2 K, (c) after  $\lambda > 380$  nm photolysis, (d) after  $\lambda > 290$  nm photolysis, (e) after  $\lambda > 240$  nm photolysis, (f) after annealing to 6.5 K, and (g) after second  $\lambda > 240$  nm photolysis.

**Figure 2.** Infrared spectra in the 1960-1760  $\text{cm}^{-1}$  region for laser-ablated Al co-deposited with isotopic hydrogen samples at 3.5 K. (a) Pure  $\text{H}_2$  and Al deposited, (b) after  $\lambda > 380$  nm photolysis, (c) after  $\lambda > 240$  nm photolysis, (d) 35%  $\text{H}_2$  + 65%  $\text{D}_2$  and Al deposited, (e) pure HD and Al deposited, and (f) after annealing to 7.3 K.

**Figure 3.** Infrared spectra in the 4500-500  $\text{cm}^{-1}$  region for laser-ablated Al co-deposited with isotopic hydrogen samples at 3.5 K. (a) Pure  $\text{H}_2$  and Al deposited and subjected to  $\lambda > 240$  nm photolysis, (b) after annealing to 6.8 K, (c) after annealing to 7.0 K, (d) Pure  $\text{D}_2$  and Al deposited and subjected to  $\lambda > 240$  nm photolysis, (e) after annealing to 14 K, (f) 40%  $\text{H}_2$  + 60%  $\text{D}_2$  and Al deposited, photolyzed  $\lambda > 240$  nm, and annealed to 13 K.

**Figure 4.** Infrared spectra in the 1440-880 and 620-500  $\text{cm}^{-1}$  regions for laser-ablated Al co-deposited with normal deuterium at 3.5 K. (a) Spectrum of sample deposited for 25 min, (b) after annealing to 7.3 K, (c) after  $\lambda > 290$  nm photolysis, (d) after annealing to 7.5 K, (e) after  $\lambda > 240$  nm photolysis, (f) after annealing to 8.0 K, and (g) after annealing to 9.0 K.

**Figure 5.** Infrared spectra in the 1950-1150  $\text{cm}^{-1}$  range for laser-ablated Al co-deposited with pure HD at 3.5 K. (a) Spectrum of sample deposited for 25 min, (b) after annealing to 6.8 K, (c) after  $\lambda > 290$  nm photolysis, (d) after  $\lambda > 240$  nm photolysis, (e) after annealing to 7.3 K, and (f) after  $\lambda > 240$  nm photolysis.

**Figure 6.** Infrared spectra in the  $1950\text{-}1550\text{ cm}^{-1}$  region of a  $1.45\text{-mm}$ -thick para- $\text{H}_2$  sample doped with  $7\text{ ppm}$  Al atoms from a thermal effusive source at  $T = 950\text{ }^\circ\text{C}$ ; sample deposition time =  $120\text{ min}$ . Trace (a) is for the as-deposited sample at  $T = 2.4\text{ K}$ , trace (b) was obtained during annealing at  $T = 4.8\text{ K}$  for about  $60\text{ min}$ , trace (c) is for the annealed sample cooled back to  $T = 2.5\text{ K}$ , and trace (d) shows the effects of irradiation with an unfiltered deuterium lamp for  $10\text{ min}$ . Spectral resolution is  $0.1\text{ cm}^{-1}$ .

**Figure 7.** Infrared spectra in the  $1950\text{-}1100\text{ cm}^{-1}$  region of a  $1.48\text{-mm}$ -thick para- $\text{H}_2$  sample doped with  $100\text{ ppm}$  Al atoms from a thermal effusive source at  $T = 1075\text{ }^\circ\text{C}$ ; sample deposition time =  $120\text{ min}$ . Trace (a) is for the as-deposited sample at  $T = 2.4\text{ K}$ , trace (b) was obtained at  $T = 2.4\text{ K}$  after irradiation with an unfiltered deuterium lamp for  $30\text{ min}$ , and trace (c) is for the sample cooled back to  $T = 2.4\text{ K}$  after annealing at  $T = 4.8\text{ K}$  for  $60\text{ min}$ . Spectral resolution is  $0.05\text{ cm}^{-1}$ .

**Figure 8.** Infrared spectra in the  $1950\text{-}1750\text{ cm}^{-1}$  region of a  $0.40\text{-mm}$ -thick para- $\text{H}_2$  sample doped with  $20\text{ ppm}$  Al atoms from a thermal effusive source at  $T = 1000\text{ }^\circ\text{C}$ ; sample deposition time =  $30\text{ min}$ . Trace (a) is for the as-deposited sample at  $T = 2.4\text{ K}$ , trace (b) was obtained at  $T = 2.4\text{ K}$  after irradiation with an unfiltered deuterium lamp for  $30\text{ min}$ , trace (c) was obtained during annealing to  $T = 4.6\text{ K}$  for  $60\text{ min}$ , and trace (d) is for the sample cooled back to  $T = 2.4\text{ K}$ . Spectral resolution is  $0.02\text{ cm}^{-1}$ .

**Figure 9.** Infrared spectra in the  $2000\text{-}1200\text{ cm}^{-1}$  range for laser-ablated Al co-deposited with neon +  $10\%\text{ H}_2$  at  $3.5\text{ K}$ . (a) Spectrum of sample deposited for  $50\text{ min}$ , (b) after annealing to  $7.0\text{ K}$ , (c) after  $\lambda > 240\text{ nm}$  photolysis, and (d) after annealing to  $7.6\text{ K}$ .

**Figure 10.** Structures calculated (B3LYP/6-311++G\*\*) for the dialanes  $\text{Al}_2\text{H}_4$  and  $\text{Al}_2\text{H}_6$ .

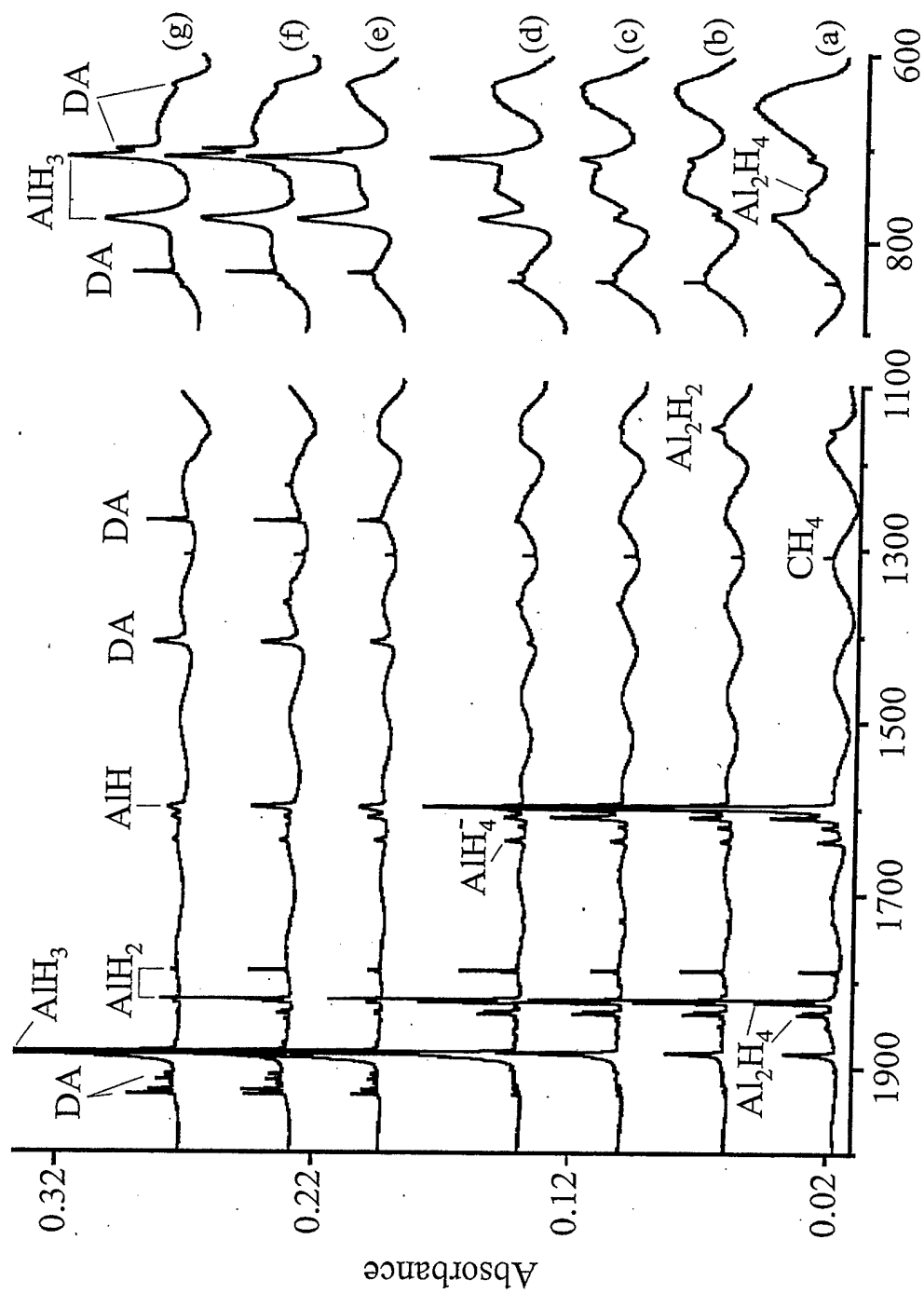


Figure 1  
Wavenumbers (cm<sup>-1</sup>)

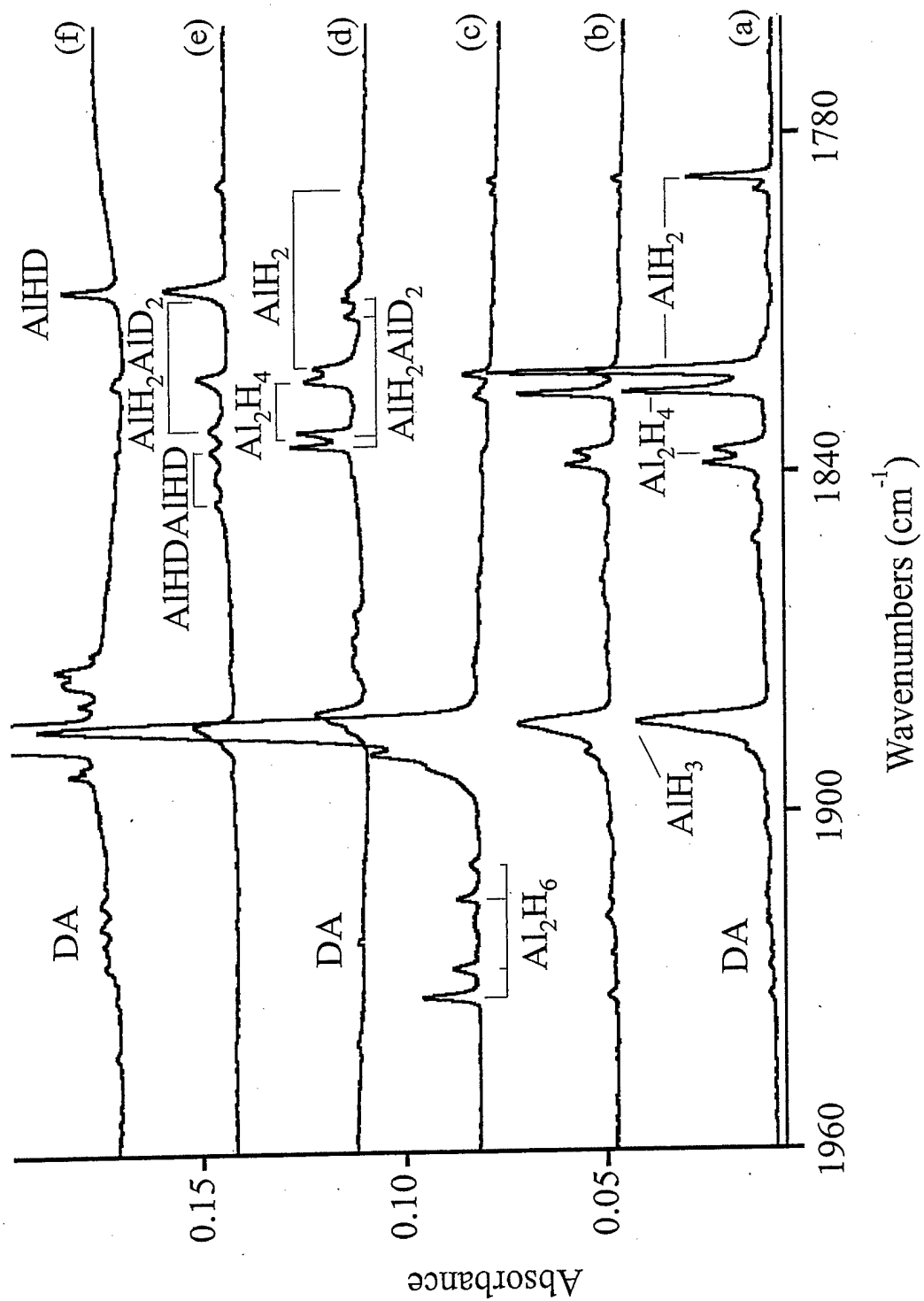


Figure 2

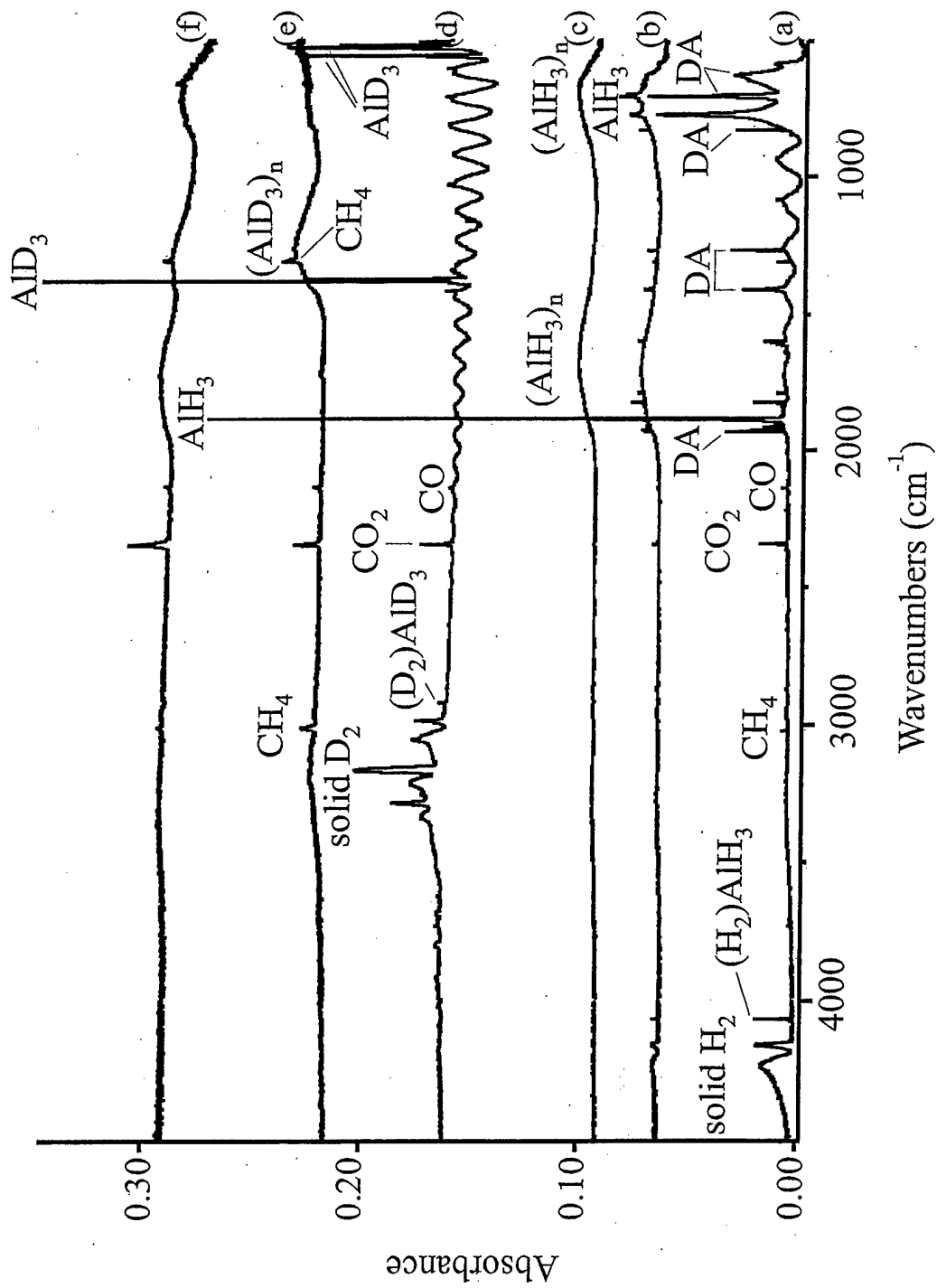


Figure 3

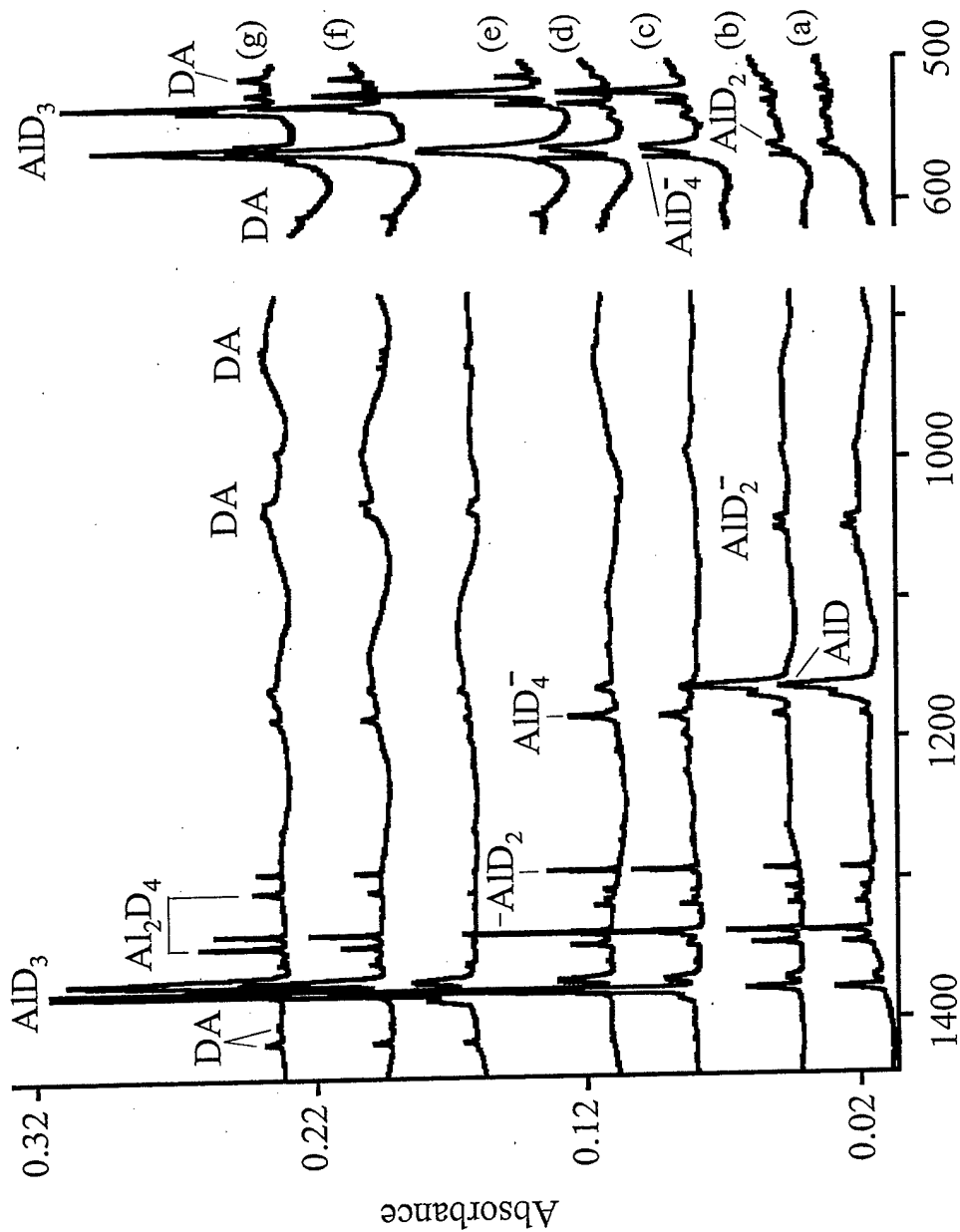


Figure 4

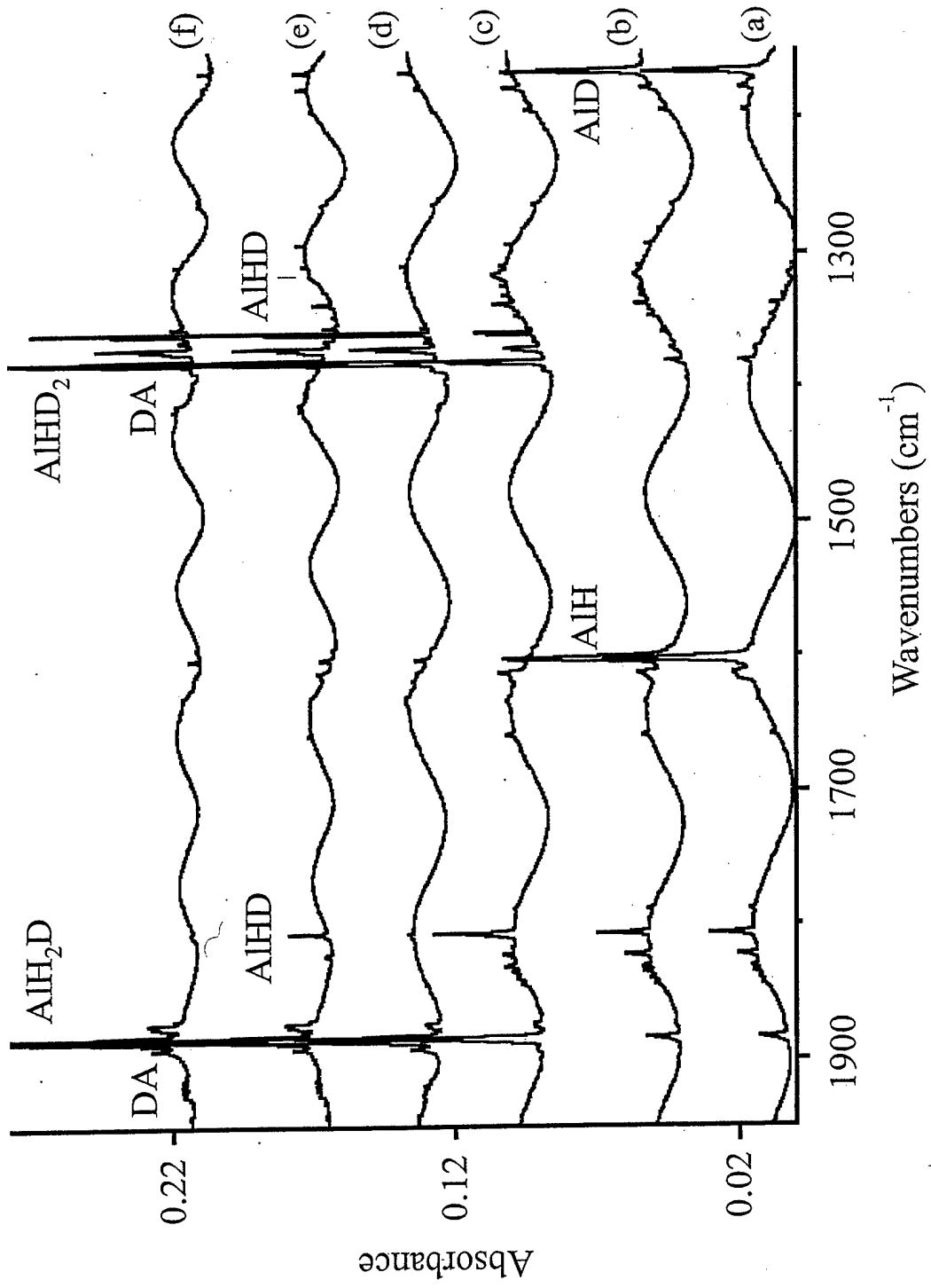


Figure 5

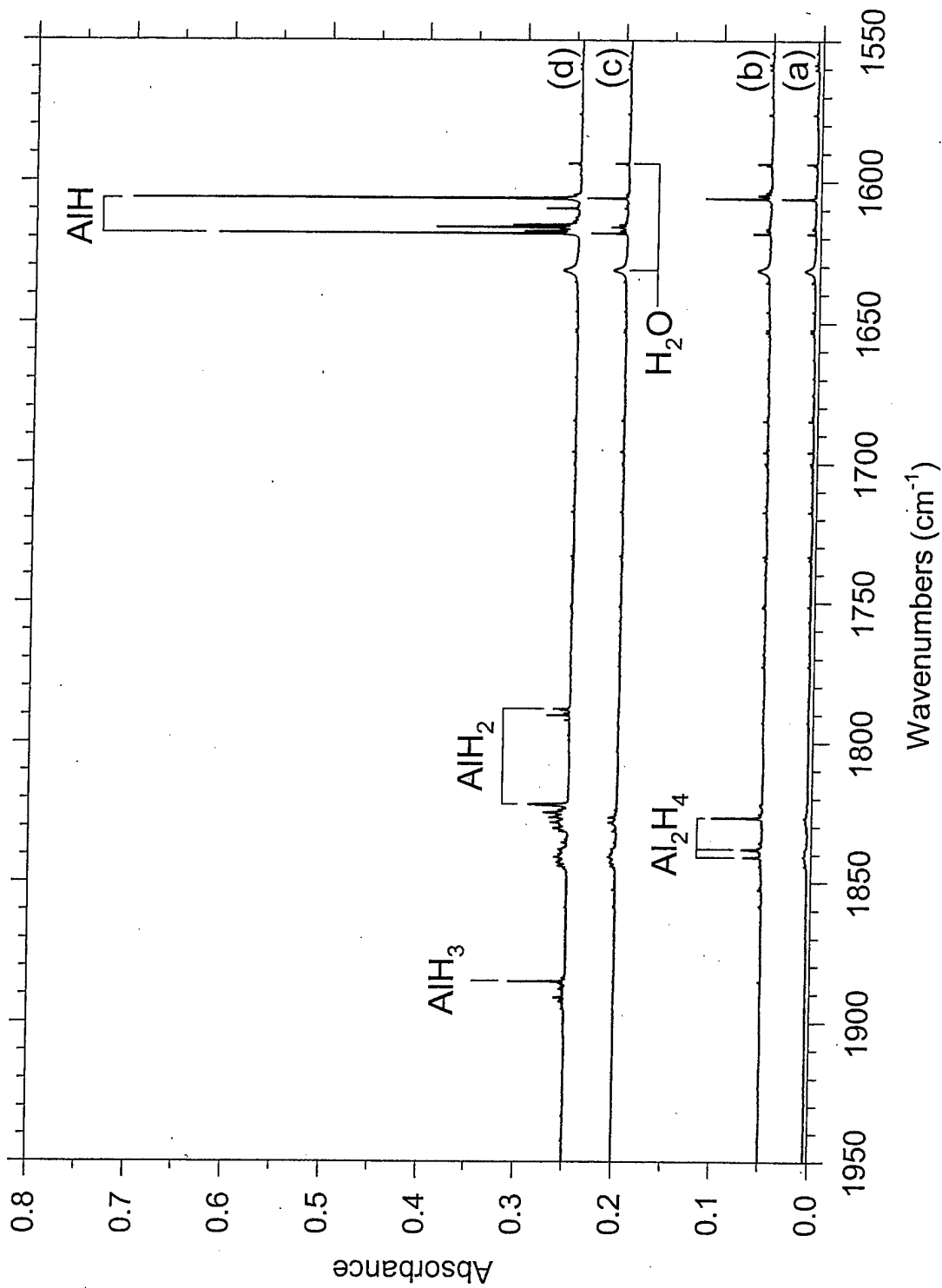


Figure 6

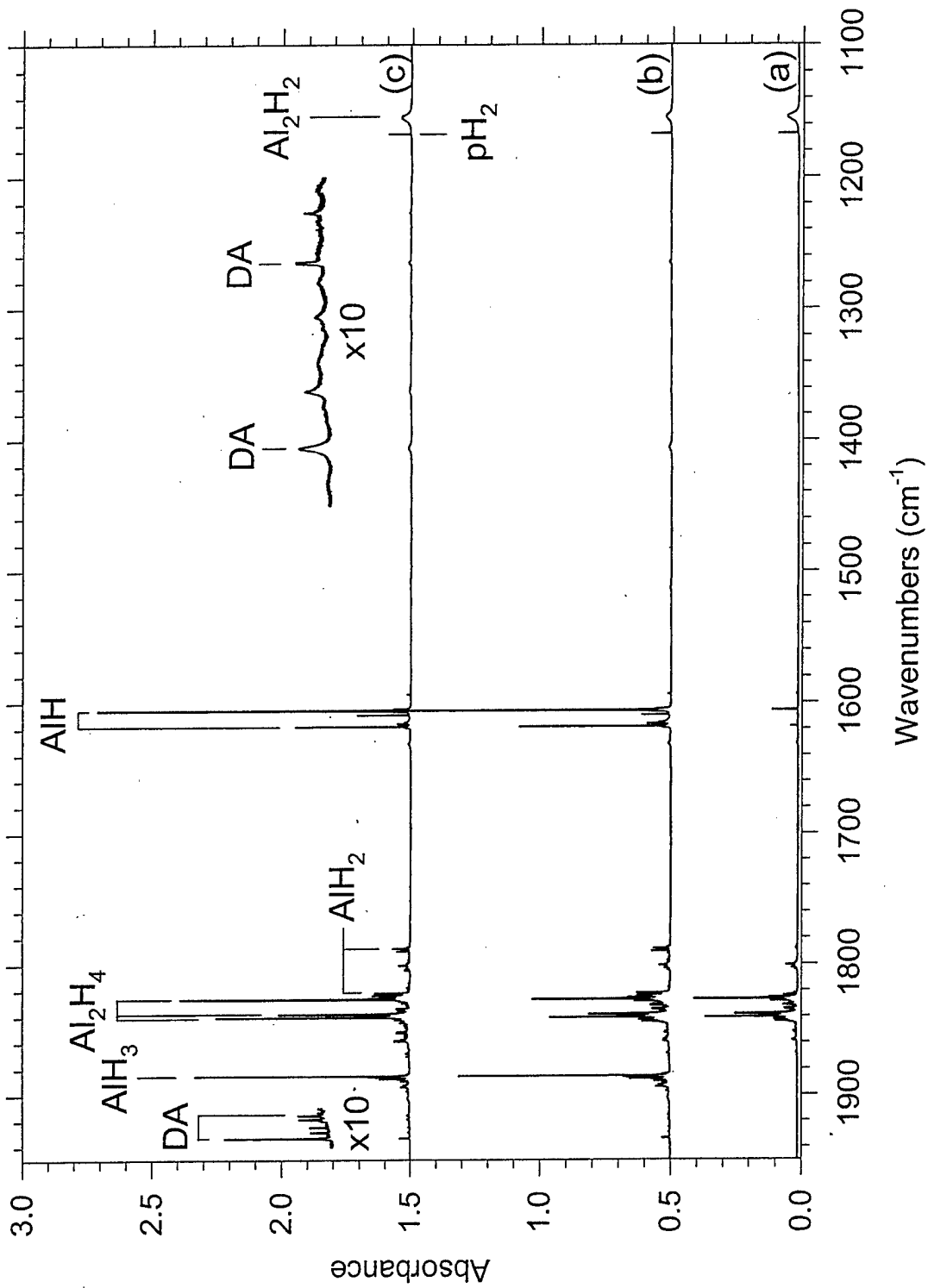


Figure 7

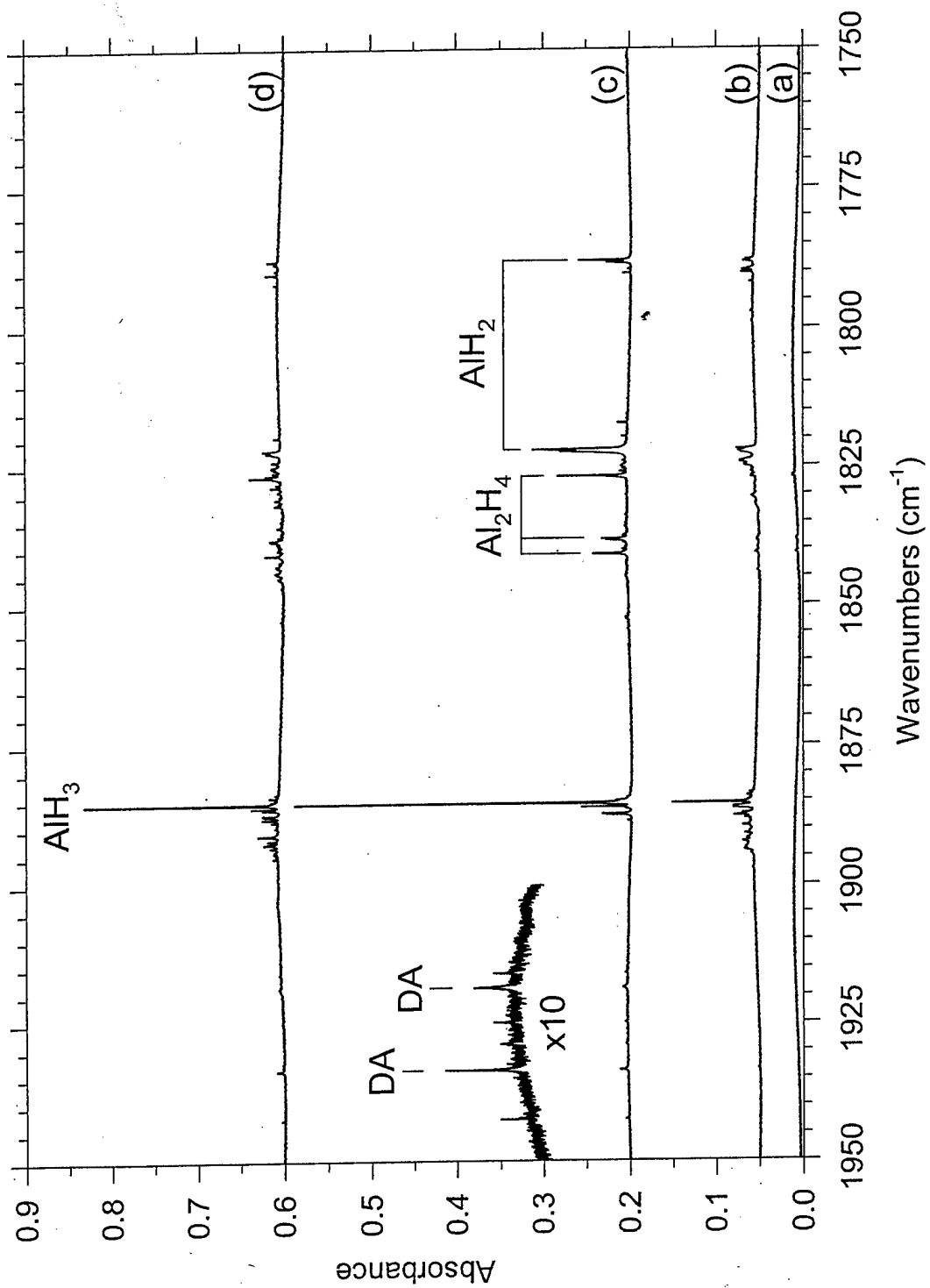


Figure 8

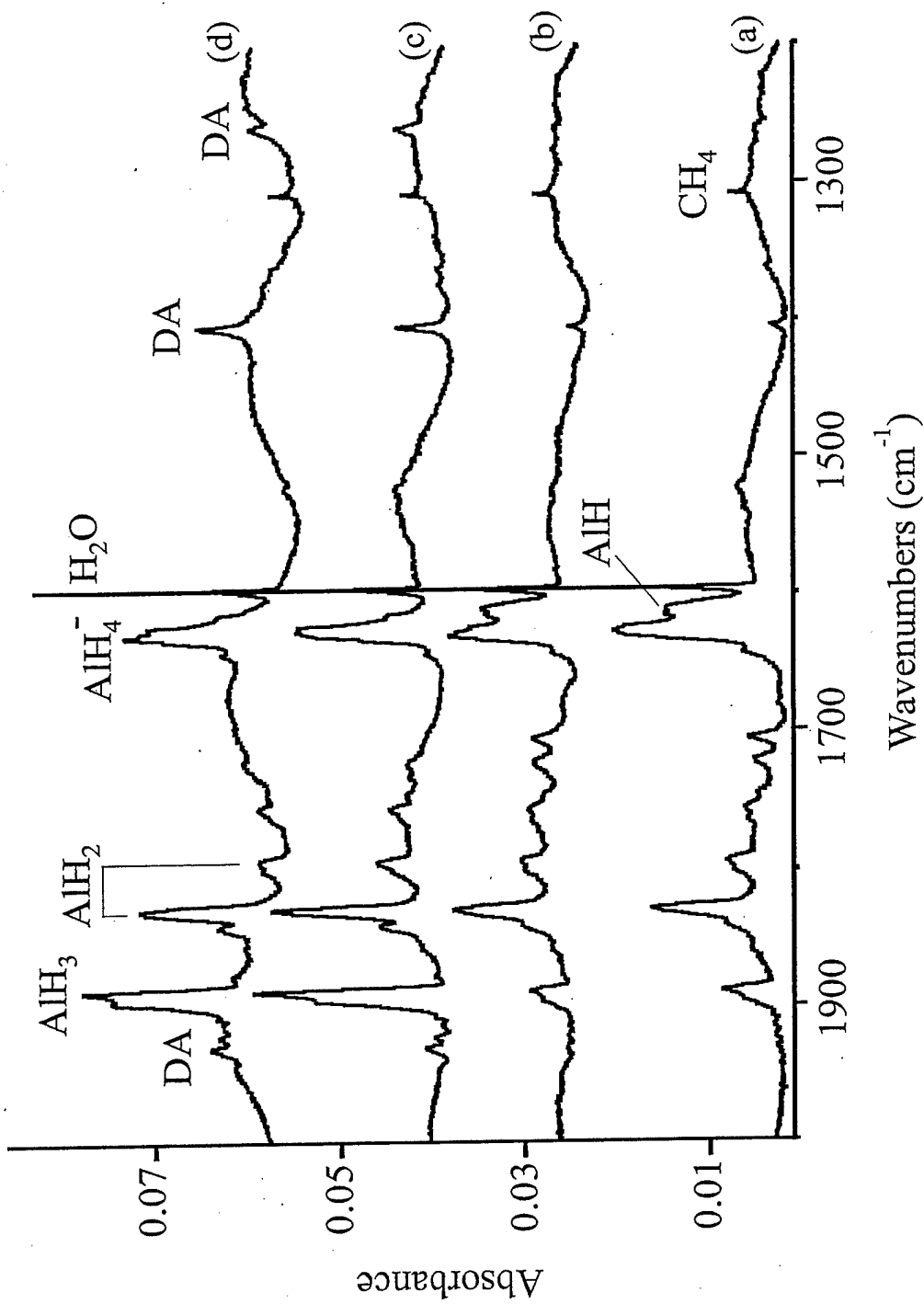


Figure 9

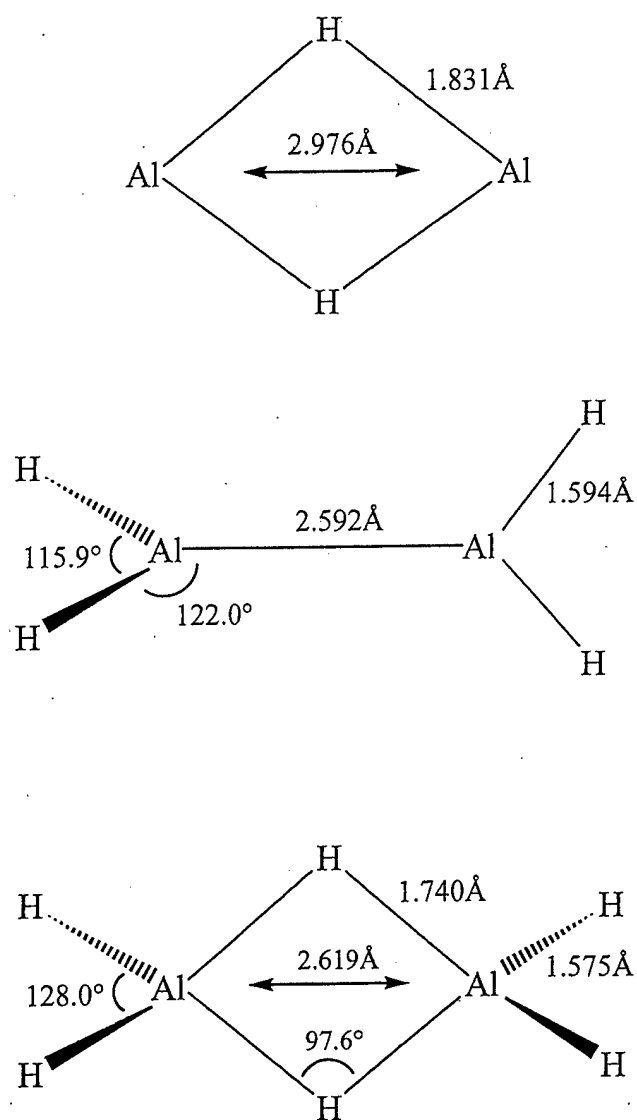
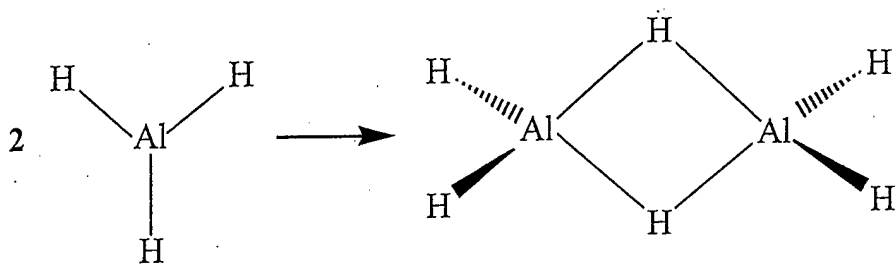


Figure 10



TOC graphics